

Stephen F. Austin State University

SFA ScholarWorks

Electronic Theses and Dissertations

Summer 8-10-2024

STRUCTURAL CHARACTERIZATION OF THE PUMA DIAPIR, GULF OF MEXICO BASIN

Rodrigo Velasquez

Stephen F Austin State University, velasquer5@jacks.sfasu.edu

Follow this and additional works at: <https://scholarworks.sfasu.edu/etds>



Part of the [Geology Commons](#), [Geophysics and Seismology Commons](#), and the [Tectonics and Structure Commons](#)

[Tell us](#) how this article helped you.

Repository Citation

Velasquez, Rodrigo, "STRUCTURAL CHARACTERIZATION OF THE PUMA DIAPIR, GULF OF MEXICO BASIN" (2024). *Electronic Theses and Dissertations*. 567.

<https://scholarworks.sfasu.edu/etds/567>

This Thesis is brought to you for free and open access by SFA ScholarWorks. It has been accepted for inclusion in Electronic Theses and Dissertations by an authorized administrator of SFA ScholarWorks. For more information, please contact cdsscholarworks@sfasu.edu.

STRUCTURAL CHARACTERIZATION OF THE PUMA DIAPIR, GULF OF MEXICO BASIN

Creative Commons License



This work is licensed under a [Creative Commons Attribution-Noncommercial-No Derivative Works 4.0 License](https://creativecommons.org/licenses/by-nc-nd/4.0/).

STRUCTURAL CHARACTERIZATION OF THE PUMA DIAPIR, GULF OF
MEXICO BASIN

By

Rodrigo Velasquez, Bachelor of Science

Presented to the Faculty of the Graduate School of

Stephen F. Austin State University

In Partial Fulfillment

Of the Requirements

For the Degree of

Master of Science

STEPHEN F. AUSTIN STATE UNIVERSITY

August 2024

STRUCTURAL CHARACTERIZATION OF THE PUMA DIAPIR, GULF OF
MEXICO BASIN

By

Rodrigo Velasquez, Bachelor of Science

APPROVED:

Dr. Julie Bloxson, Thesis Director

Dr. Wesley Brown, Committee Member

Dr. Zachariah Fleming, Committee Member

Dr. Jenny Rashall, Committee Member

Forest Lane, Ph.D.
Dean of Research and Graduate Studies

ABSTRACT

The Gulf of Mexico (GOM) Basin has been a significant target for oil and gas since the 1990s and continues today as a leading exploration target. This super basin is home to an estimated 200 BBOE (Billion barrels of oil equivalent), with current production totaling 60 BBOE for both USA and Mexico. Even though the overall depositional evolution of the GOM has allowed for the key elements for petroleum accumulations to be met, a complex structural framework is present. This framework results from the asymmetric spreading of the North American Plate from the Yucatan block crating the GOM basin we see today, coupled with Jurassic Louann Salt deposits precipitated throughout the basin. The subsequent increasing sedimentary load created complex gravity-induced tectonic structures, resulting in various salt stocks and canopies forming in the Louann Salt.

This research aims to characterize the structure surrounding the Puma Diapir, located in the southeastern region of the Green Canyon Protraction of the Gulf of Mexico. The seismic dataset is a multiclient 3D depth survey from WesternGeco that combines wide azimuth acquisition (WAZ) and full azimuth acquisition (FAZ) datasets to produce a final image. The base and top of the salt in our study area are carefully mapped using the Kingdom Suite software. These structure maps are used as a visual aid in accessing the structural framework of the salt dome. Within the Puma Diapir, there

are two salt feeders into the canopy. Above the allochthonous salt sheet, we find secondary bucket-style minibasins, where the strata are sinking into the underlying salt feeders. The area consists of a variety of normal faults, and reactive salt structures. Above the salt dome, shallow extension faulting is the result of the rising body. Overall, the Puma Diapir shows classic, yet complex structural features associated with salt movement.

ACKNOWLEDGMENTS

I would like to thank my thesis committee, Dr Zach Fleming, Dr. Wesley Brown, and Dr. Jenny Rashall for their guidance and support. A huge thank you to Dr. Julie Bloxson for the continuous support and knowledgeable feedback. I would also like to thank my family for the motivation and support. To my close friends for the patience and long nights that were crucial to successfully completing my thesis. And a special thanks to WesternGeco for the seismic data that made this research possible.

TABLE OF CONTENTS

ABSTRACT.....	III
ACKNOWLEDGMENTS	V
TABLE OF CONTENTS	VI
LIST OF FIGURES	VIII
LIST OF TABLES	XII
1.INTRODUCTION.....	1
2.SALT TECTONICS.....	5
3.STUDY AREA AND PREVIOUS PUMA DIAPIR STUDIES	9
3.1 MINIBASIN	10
3.2 MEGAFLAP	12
3.3 SALT FEEDER	13
3.4 SALT WELDS	14
4.TECTONIC FRAMEWORK	15
5.STRATIGRAPHY	19
5.1 LOUANN SALT.....	22
5.2 NORPHLET FORMATION.....	22
5.3 MIOCENE – PLIOCENE	23
5.4 MOBILE SHALE	25
6. METHODS	27
7. RESULTS	33
7.1 HORIZONS	33
7.2 MINIBASINS.....	36
7.2.1 <i>Minibasin 1</i>	40
7.2.2 <i>Minibasin 2</i>	41
7.2.3 <i>Minibasin 3</i>	43
7.2.4 <i>Minibasin 4</i>	45
7.2.5 <i>Minibasin 5</i>	46
7.2.6 <i>Minibasin 6</i>	48
7.3 MEGAFLAPS PUMA DIAPIR.....	51
7.4 SALT FEEDER PUMA DIAPIR.....	53

7.5 SALT WELDS PUMA DIAPIR	55
7.6 SALT BODY	56
7.7 FAULTS	59
7.8 FRONTAL THRUST SYSTEMS.....	62
7.9 MOBILE SHALE	65
8. DISCUSSION	69
8.1 PUMA DIAPIR EVOLUTION.....	69
9. CONCLUSIONS	79
10.REFERENCES.....	82
11.VITA.....	88

LIST OF FIGURES

Figure 1. Distribution of Callovian salt across the Gulf of Mexico basin after extensional rift tectonics between the Yucatan micro plate and the North American Plate (Hudec et al., 2013)	2
Figure 2. Representation salt influenced basin geometries in the deep-water Gulf of Mexico. Black represents salt. Primary basin shaded in grey. Secondary basins in white. Red lines outline the general basin geometry type and style for the study. Modified from Pilcher et al., 2011.	3
Figure 3. Diagram of different types of salt structures resulting from halokinesis. From Fossen (2010).	6
Figure 4. (A) Autosutures form by overriding itself, creating “folds” in the salt body and incorporating strata, while (B) asymmetric allosutures form by overriding another salt body, incorporating strata. Modified from Dooley (2012).	8
Figure 5. Study area location in the offshore Gulf of Mexico Basin off the Louisiana shoreline (outlined in red). Bathymetry shows the salt diapir influencing the bedrock strata. Bathymetry from BOEM (2024).	9
Figure 6. 3D post stacked depth migrated seismic line from the northern Gulf of Mexico illustrates the location of primary and secondary (supra-salt) minibasins, salt welds and expulsion rollover. Seismic unit overturning and thinning towards the base of the salt canopy creates a megaflap. Modified from Hearon et al. (2013).	13
Figure 7. Plate reconfiguration and salt deposition during the GOMB formation throughout the Late Triassic to modern day. Modified from Jackson et al. (2013).	18
Figure 8. General North-South cross section of the Gulf of Mexico and its complex relation between the salt (black) and intraslope sediments. Modified from Fisher et al. (2007).	20
Figure 9. Stratigraphic column of the northeastern Gulf of Mexico. Formations of interest are outlined in red. Modified from Mattson et al. (2020).	21
Figure 10. Depth map to the top of the Mobile shale created in Kingdom Suite.	26
Figure 11. (A) Gulf of Mexico Basin with protraction outlined in blue showing the area of interest (AOI) and (B) a close up of the AOI with the 3D seismic grid.	27
Figure 12. Grid of seafloor reflector from 3D post migrated data Kft from sea level.	32

Figure 13. Inline 6541. The lower shaded grey is the autochthonous salt, upper is the salt canopy. Horizons mapped throughout the data set. Top Cretaceous (T1), Top Paleocene – Eocene (T2), Top Oligocene (T3), Lower Miocene (T4), Middle Miocene, Upper Miocene (T5), Recent – Top Pleistocene (T6).....	36
Figure 14. Depth map (depth below sea level in Kft) for top salt, showing the overall salt-tectonic structure of the study area with the impression of the five secondary minibasins on the top of the salt canopy. The location of the primary minibasin (MB6) is not shown.	38
Figure 15. Time slice of data @ 6.6 [twts] truncation the secondary minibasin. Location of seismic lines used in seismic unit horizons. Line A ((Figure 15), minibasin 1), Line B ((Figure 16), minibasin 2), Line C ((Figure 17), minibasin 3,), Line D ((Figure 18), minibasin 4), Line E ((Figure 29), minibasin 5).	39
Figure 16. Seismic section of minibasin 1. Location of this line (Line A) is shown in Figure 15. Minibasin 1 consists of a bowl shaped minibasin with a welded base. (white arrow), draping of strata against the salt (orange arrow), and thinning of overlying strata (green arrow). The 3 MTC found are shaded and outlined (yellow arrows).	41
Figure 17. Seismic section of minibasin 2. Location of this line (Line B) shown in Figure 15. The elongated basin has four MTC that thin towards the salt high. (white arrows), localized zone of mobile shale (orange arrow), chaotic top of salt with no visible mobile shale (blue arrow).	43
Figure 18. Seismic section of minibasin 3. Location of this line (Line C) is shown in Figure 15. One MTC found in the lower units of the basin. (white arrow pointing to shaded area of MTC unit). Areas of rough salt surface located under the mobile shale with increased internal seismic reflectors (blue arrows), seismic units displaying syn depositional shape as they thin over the salt high (yellow arrow).	44
Figure 19. Seismic section of minibasin 4. Location of this line (Line D) is shown in Figure 15. Large mobile shale unit in shaded purple (white arrow), roof edge thrust created by the shortening event on the canopy edge (orange arrow), seismic units onlapping and thinning towards the salt high (blue arrow).	46
Figure 20. Seismic section of minibasin 5. Location of this line (Line E) is shown in Figure 15. Four MTC systems are seen to thin towards the NE (white arrows). The eroded top surface of SU6 outlines the base of the channel (yellow arrow). Top and bottom reflectors of the inclusion found within the salt canopy (blue arrows).	48
Figure 21. Time slice @ 30 [Kft]. Shaded dark grey area is the salt feeder limits, and red line (white arrows) outlines the extent of the primary minibasin.	50
Figure 22. Minibasin 6. Location of the line (Line F) in Figure 21. Seismic Horizons, T1– Top Cretaceous. T2 – Top Paleocene – Eocene. T3 – Oligocene. T4 – Top lower	

Miocene. T1 – T4 seismic units thin and onlap the flanks of the salt feeder (blue arrows). Sutures located in the salt canopy (green arrows). White arrows denote direction of salt movement.....	51
Figure 23. Section from Kingdom suite software in 3D post migrated data. White arrows pointing to the base autochthonous salt. Yellow arrows pointing to T1 and T2 seismic units. The units are overthrusting creating a megaflap. Blue arrow pointing to base of the salt canopy. Section from Kingdom suite software in 3D post migrated data.....	52
Figure 24. Top of salt canopy limits in the AOI. Seismic units 1 and 2 are located under the salt canopy (yellow arrow). The base salt is the lower most and is the bottom surface for the megaflap (white arrow).	53
Figure 25. Salt Feeder limits, Horizon 1 light yellow, Horizon 2 in golden yellow. Feeder Horizon 1 was used to map the lower flanks until the limits of the horizon tool were met, at which Feeder horizon 2 was used to map the upper limits of the near vertical salt.	54
Figure 26. Map showing depth in time to the base of salt canopy, that was mapped on the soft reflector across the dataset interpreted to be the base of the salt. The area labeled salt feeder outlines the point at which the salt is dipping downward, and no longer parallels the sea floor.....	55
Figure 27. Salt in shaded grey area. Location of welds visible in our data set, noted by the two white dots.	56
Figure 28. Map of top of the salt canopy in Kft. Approximate location of Salt Body A is outlined in blue and located in the southwestern portion of the study area. Salt Body B is outlined in red and located to the northeast.	58
Figure 29. Cubic Volume of 3D seismic, the extent of viewed section is outlined in yellow within the AOI. Seismic has been reprocessed to enhance relief of the reflection surfaces. The base of the salt canopy (white arrows) is easily distinguished from the underlying reflectors with the enhanced reflection. Salt body A is encountering the Salt body B, creating a basal suture point (blue arrow). Internal salt reflectors at the top of the time slice are identified by the green arrows.	59
Figure 30. Distribution of faults located above the salt canopy (white arrow). (A) Plane view of AOI with faults. (B) View facing the west side of the data set where the limit of the salt canopy shown. The red line is an approximate location where the top salt body meet.....	61
Figure 31. Regional 3D time migrated data, salt limits outlined in shaded grey. Strike-slip system is located towards the seafloor on the southwestern end of the seismic profile (white arrow). Reflectors within the salt canopy denote sutures (blue arrows). Salt diapir pedestal located under the allochthonous salt (yellow arrow).	61

Figure 32. Rose diagram from generated by Kingdom Suite using the faults mapped in the dataset. Diagram shows dominate strike trend for the faults, and dip.	62
Figure 33. Salt body A to the left Salt body B to the right, Roof-edge thrust towards sea floor (blue arrow). Echelon extensional faulting is found above salt body A (yellow arrow). The inclusion found in salt body A is easily distinguished from the seismically transparent salt (white arrow).	64
Figure 34. Shaded Purple defines transparent mobile shale. Shades grey marks the extensional salt rollover note prominent roof thrust (blue arrow) system toward the southeast. There is a seismically transparent zone underneath the tip of the roof thrust (yellow arrow). Sediment accumulation occurs in front of the thrust (white arrow).	65
Figure 35. Limit of mobile shale found above the salt canopy. The shale is found mostly in the lows from rising salt.....	66
Figure 36. Line 6501. Areas with lower amounts of mobile shale shaded in purple (blue arrows) correlate with increased amounts of intra salt reflections (yellow arrows) identified as sutures.....	67
Figure 37. Diagram of the Puma Diapir during the Cretaceous, showing passive diapirism. The massive Louann Salt was deposited over preexisting basement rock during the Middle Jurassic (Bajocian; ~162-163 Ma (Hudec et al., 2013)).....	71
Figure 38. Diagram showing active diapirism during the Paleocene-Eocene. T1 – Cretaceous; T2 – Paleocene – Eocene. The increased sediment loading is the driving mechanism for salt motion during this time. Top of Paleocene – Eocene unit conformably overlying the Cretaceous units.....	72
Figure 39. Diagram showing reactive diapirism during the Oligocene. T1 – Cretaceous; T2 – Paleocene – Eocene. T3 – Oligocene.	73
Figure 40. Passive – active diapirism (lower – middle Miocene depositional episodes) Diagram illustrating passive diapirism in the Puma Diapir during the Miocene depositional episodes. T1 – Cretaceous; T2 – Paleocene – Eocene. T3 – Oligocene. T4 – Miocene.....	75
Figure 41. Diagram illustrating active diapirism during the upper Miocene. T1-T4 has become an encased minibasin, active diapirism forceful intrusion into overlying strata salt as sedimentation continues. Salt body A contacts salt body B, and the creation of basal suture commences. T1 – Cretaceous; T2 – Paleocene – Eocene. T3 – Oligocene. T4 – Miocene. T4 – Pleistocene.	76
Figure 42. Diagram illustrating the modern structure of the Puma Diapir, undergoing active diapirism. T1 – Cretaceous; T2 – Paleocene – Eocene. T3 – Oligocene. T4 – Lower Miocene / Middle Miocene. T5 – Upper Miocene. T6 – Pleistocene – Recent. ...	78

LIST OF TABLES

Table 1. Acquisition parameters for EDGE survey (Courtesy of WesternGeco).....	30
--	----

1.INTRODUCTION

The Gulf of Mexico (GOM) Basin has been a significant oil and gas target since the 1990s and continues today as a leading exploration target. This super basin is home to an estimated 200 BBOE (Billion barrels of oil equivalent), with current production totaling 60 BBOE for both the USA and Mexico (Snedden and Galloway, 2019). The complex structural framework and depositional evolution of the GOM basin has allowed for all the key elements for petroleum accumulations to be met. This framework results from the asymmetric spreading of the North American Plate from the Yucatan block creating the GOM basin we see today coupled with halokinesis (Figure 1) (Galloway, 2008). Furthermore, during the Middle Jurassic (Callovian), widespread sheets of thick salt deposits (upwards of 4 km) known as the Louann Salt precipitated throughout the basin. The subsequent increasing sedimentary load created complex gravity-induced tectonic structures, resulting in various salt stocks and canopies forming in the Louann Salt. (Hudec et al., 2013).

The northern GOM has one of the most complex assemblages of gravity tectonics affecting the surface and subsurface geology. The resulting salt structures create two types of minibasins, primary and secondary. They are distinguished from one another by the following criteria: Primary minibasins are located under allochthonous salt, most of the strata are bounded by salt on all sides and have a welded base. Secondary minibasins

are found above the salt canopy (Peel, 2014) (Figure 2). A mixture of the extremely thick Louann salt and rapid sediment loading has caused the massive Louann Salt to Mobilize across the basin (Ewing and Galloway, 2019).

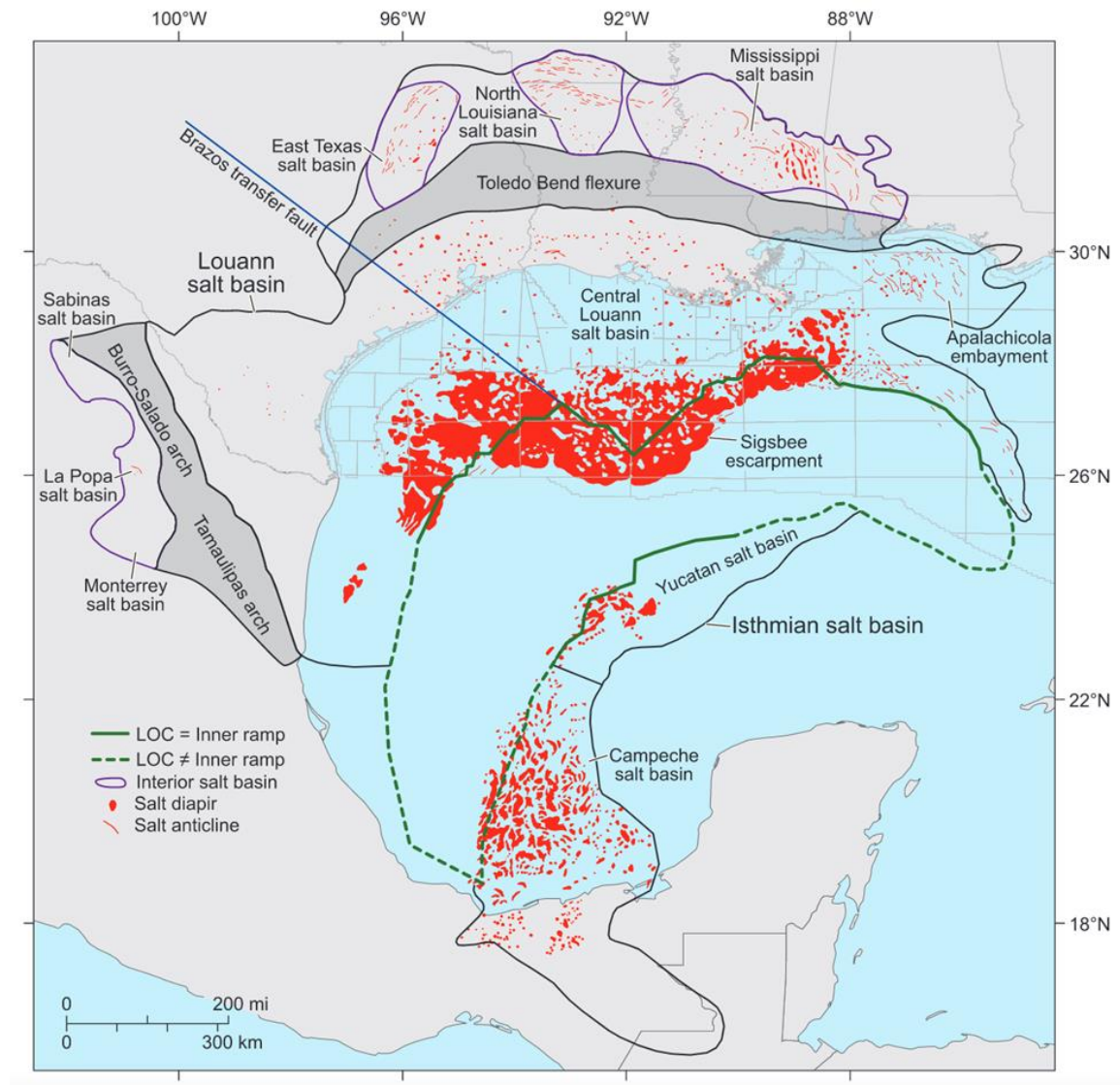


Figure 1. Distribution of Callovian salt across the Gulf of Mexico basin after extensional rift tectonics between the Yucatan micro plate and the North American Plate (Hudec et al., 2013)

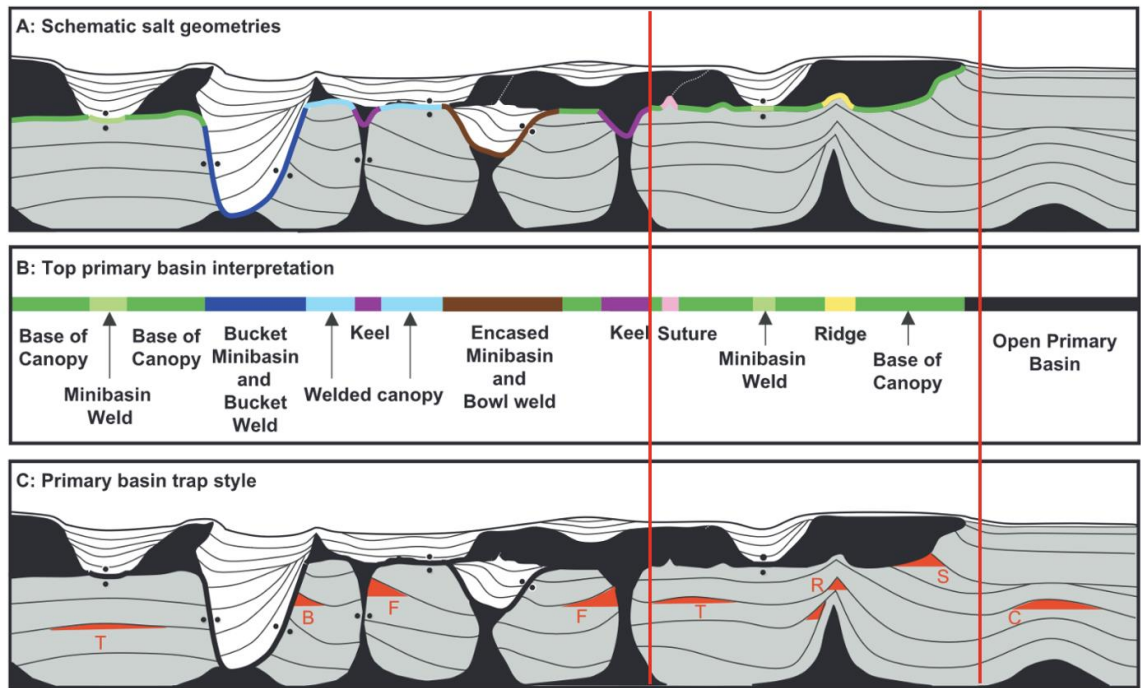


Figure 2. Representation salt influenced basin geometries in the deep-water Gulf of Mexico. Black represents salt. Primary basin shaded in grey. Secondary basins in white. Red lines outline the general basin geometry type and style for the study. Modified from Pilcher et al., 2011.

Sediment loading of the Louann Salt has resulted in regional extrusion of salt towards the basin and up section (Ewing and Galloway, 2019). By the Late Cretaceous, much of the salt had been reworked towards the basin by overlying pelagic and siliciclastic deposition. A layer of autochthonous salt provides a surface for the overlying strata to be mobilized due to gravity loading. Miocene-Pliocene deposition over the salt canopies caused passive diapirism and further gravity spreading (Ewing and Galloway, 2019). The mobilization of younger salt into or on top of younger stratigraphic levels is

referred to as allochthonous salt (Hearon, 2013). Mobilization influences the structure of the surrounding strata, causing folding, faulting, doming, and sinks throughout a region. This work will assess the Puma Diapir, located in the Green Canyon Protraction near the Atwater fold belt, to better understand the interaction between the Louann and surrounding strata.

This research aims to characterize the structure surrounding the Puma Diapir, which is located near the Sigsbee Escarpment in the Gulf of Mexico basin. 3D seismic has been acquired over the diapir, allowing for accurate characterization of the structure in the region. The structural characterization of the area is beneficial to many aspects of geology, specifically the subsurface understanding of how large evaporite bodies influence the surrounding strata through time. After the structural evaluation of the Puma Diapir and associated strata, the results and models can be used to compare surrounding diapirs or similar allochthonous salt bodies along with their seismic interpretation. This study will also increase accuracy when mapping subsurface faults, specifically the extent and relation to other faults. Regarding oil and gas exploration, a better understanding of salt tectonics and associated geophysical seismic interpretation can lead to a better understanding of hydrocarbon migration, traps, reservoir size, and capacity.

2.SALT TECTONICS

Salt is defined as any rock composed chiefly of halite, although most salt bodies, like the Louann, contain other minerals such as anhydrite and gypsum (Hudec and Jackson, 2007). The unique properties of salt cause it to be relatively unstable in certain conditions. Evaporites under geologic conditions cause salt bodies to behave viscoelastically, whereas, under typical strain rates, salt flows like a fluid in the subsurface. As a result, salt bodies form a variety of salt structures (Figure 3). Salt is also rather incompressible; this, paired with a low density when compared to the clastics sediments found near it, makes the salt bodies buoyant under certain depths (Hudec and Jackson, 2007). Salt tectonics and current-day interpretations of salt stress the importance of differential loading as the main mechanism in salt flow. Three types of loading drive salt flow: gravitational loading, displacement loading, and thermal loading. Buoyancy was also once considered the main factor in initiating diapirism and is still found to be important in certain areas (Hudec and Jackson, 2007). Structures located above the salt usually include thrusts and narrow box fold anticlines in areas with regional shortening (Hudec and Jackson, 2007).

Allochthonous salt is defined as a sheet-like body of mobilized evaporite or layered evaporite sequence located at younger stratigraphic levels above the original autochthonous source (Hudec et al., 2011; Hearon, 2013). The allochthonous bodies can

result from a single salt feeder or various feeders that place salt sheets or salt tongues above the younger strata. The composite structure is formed through the coalescence of two or more salt sheets from salt canopies (Jackson and Hudec 2017). A salt sheet is an allochthonous salt sourced from a single feeder. The structures are a result of the interaction between sediment accumulation rate and salt rise rate (Giles and Rowan, 2012).

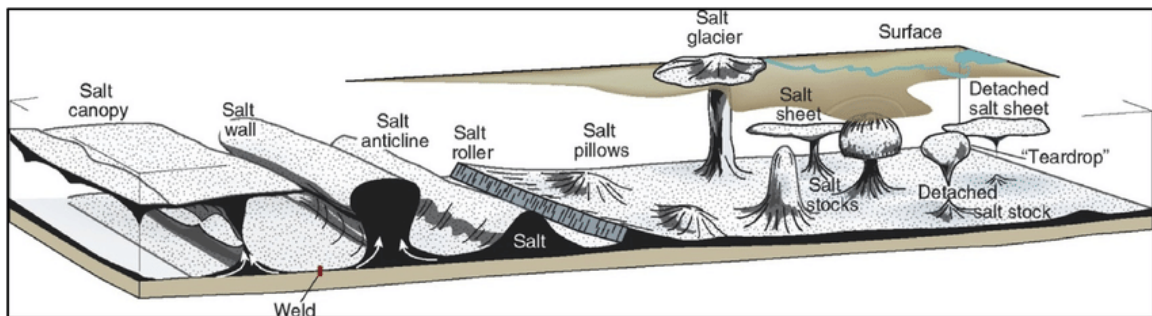


Figure 3. Diagram of different types of salt structures resulting from halokinesis. From Fossen (2010).

Salt is the weak point in most rock systems where evaporites are present, causing salt tectonics to be closely linked to regional deformation (Hudec and Jackson, 2007). Salt diapirs are the dominant structure associated with regional extension, their overall shape and size are dependent on salt availability to feed the diapir. Low relief structures such as salt rollers and listric growth faults are characteristic of extensional systems. Salt structures can be associated with regional shortening systems as well such as convergent plate boundaries and inverted rift basins (Rowan et al., 2004), but the increased thickness

of the overburden makes it difficult for diapirs to form. However, salt in these systems can become a decollement surface that can result in certain areas being dominated by thrust and narrow box fold anticlines (Hudec and Jackson, 2007).

Furthermore, sutures form within the salt bodies with constant loading and movement. Sutures are zones separating two coalesced salt sheets or two lobes of a single salt sheet, which often include sediment inclusions (Dooley et al., 2012). These sutures can then be further divided into allosutures, where two different salt bodies from different feeders come in contact, and autosutures, where the salt that is in contact is from the same salt bodies (“rollover”) (Dooley et al., 2012). Allosutures typically result when the sedimentation rate is higher than the advancement of the salt sheet. A defining feature of allosutures can be seen in the lowermost suture, which should be located along a structural high in the base of the salt; also, the majority of allosutures are produced when one of the salt sheets overrides the other (Dooley et al., 2012). Autosutures are usually found with smaller shortening structures that parallel the suture. Autosutures can be recognized by their resemblance to imbricate thrust sheets when produced by the process overriding (Dooley et al., 2012). They are recognized to be produced by encircling – when a subtle high is seen as the sediments accumulate and the salt body surrounds it (Figure 4). As these sutures form, the incorporation of sediments and the resulting pressures create an area of risk for drilling situations. Accurate identification of the suture types leads to a better overlying strata assessment and reduces drilling hazards (Hapnes 2014).

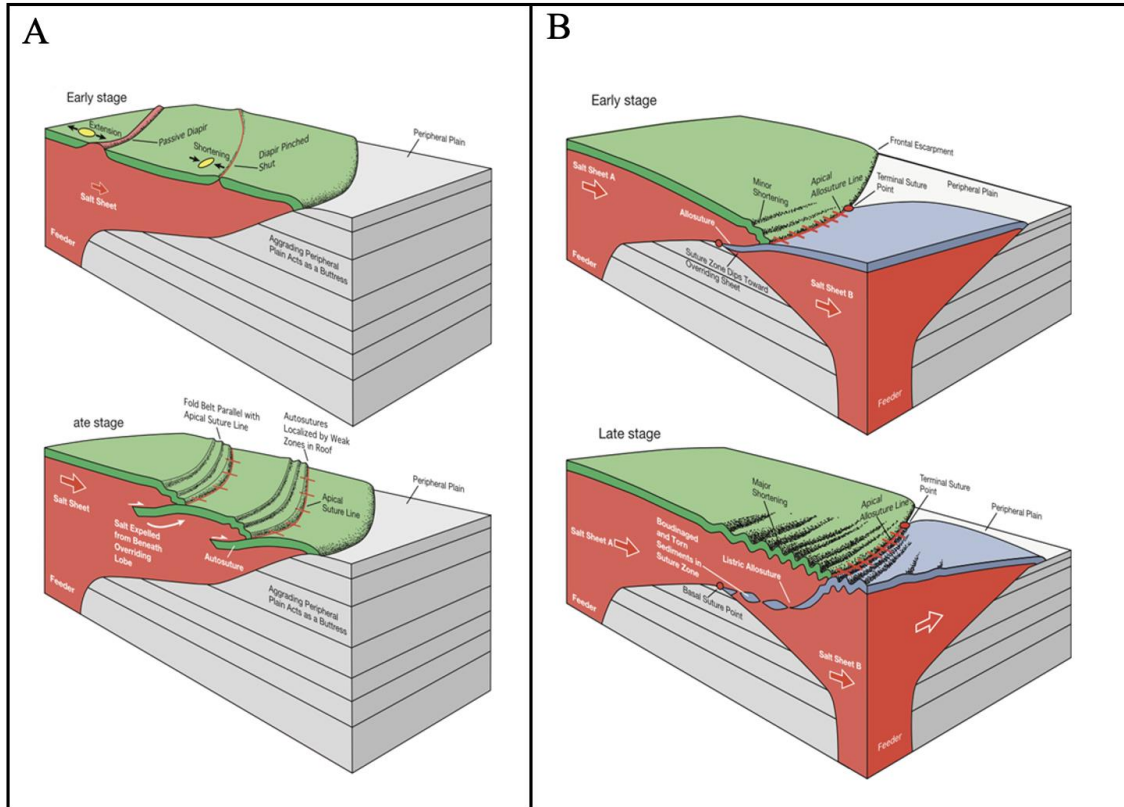


Figure 4. (A) Autosutures form by overriding itself, creating “folds” in the salt body and incorporating strata, while (B) asymmetric allosutures form by overriding another salt body, incorporating strata. Modified from Dooley (2012).

3. STUDY AREA AND PREVIOUS PUMA DIAPIR STUDIES

The study area is in the Puma Field within the Southern Green Canyon protraction of the northern GOM within the Atwater fold belt (Bowling, 2009) (Figure 5). BP discovered the Puma Field in January 2004, and the nearby Mad Dog Field was discovered earlier in November 1998. These two fields are located approximately 140 miles (225 km) south of the Louisiana coastline (Bowling, 2009).

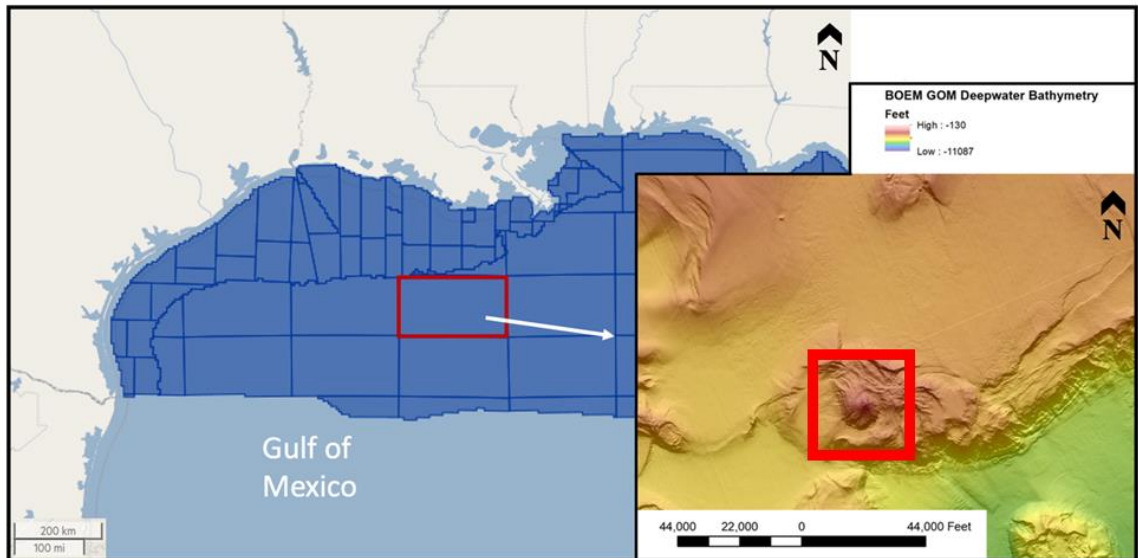


Figure 5. Study area location in the offshore Gulf of Mexico Basin off the Louisiana shoreline (outlined in red). Bathymetry shows the salt diapir influencing the bedrock strata. Bathymetry from BOEM (2024).

A previous study at the Puma appraisal area looked at the biological relationship that resulted from the salt diapir affecting the seafloor and its relation to the

chemosynthetic communities (Weiland, 2008). The study described the area of the Puma salt structure as containing large faults originating from the top of the salt that extends to the seafloor, forming a series of bathymetric ridges along the structure's north side (Weiland, 2008). They also described the area as being extensively tilted and thinned, which caused faulting in the strata above the salt. The faulting created migration pathways of asphalt, oil, and gas to the seafloor (Weiland, 2008).

A second recent study focused on a geochemical variation of the Puma Diapir. The study used XRF and XRD on the cuttings from the Puma West GC821-002 well (Lesh, 2022). Using the data obtained from the geochemical analysis, they were able to determine the elemental composition of the allochthonous Louann Salt, were able to show the bulk lithology for the well cuttings and describe the relationship between the elemental composition of areas outside and within the suture zone that of the well penetrated (Lesh, 2022). The study determined that salt is composed primarily of magnesium, silicon, sulfur, chlorine, and calcium. The suture zone varied in composition with increasing concentrations of silicon, aluminum, and potassium. The detailed analyses and proper determination of suture types from the research by Lesh (2020) will aid in an accurate interpretation of the structures surrounding the diapir.

3.1 Minibasin

A minibasin is a synkinematic basin subsiding into relatively thick, allochthonous or autochthonous salt (Jackson and Talbot, 1991; Callot et al., 2016). The development of a mini basin can be described in three main phases: 1) depocenter initiation and

proceeding avulsions, 2) the down-building phase, and 3) collapse or death of the basin occurs due to basal contact (Callot et al., 2016). The encasement of the original minibasins by salt is a primary minibasin. Secondary minibasins are created as sedimentation occurs above a salt sheet or salt canopy and the proceeding down building into the allochthonous salt leads to the development of secondary basins (Callot et al., 2016). The interaction between the development of primary and secondary basins results in salt welds and tectonic deformation at basin boundaries. Primary minibasins are distinguished from secondary minibasins by the following criteria: they are located under allochthonous salt, and most of the strata are bounded by salt on all sides and have a welded base.

Imaging primary minibasins proves to be challenging, especially in regions where the basin is overlain by a thick salt canopy. The complex geometries are poorly imaged which has led interpreters to rely on petrophysical log data and laboratory-scale models. Mattson (2019) mapped the spatial distribution of a salt canopy and showed three distinct levels of salt in the northern Gulf of Mexico. The distribution of these layers correlates with the placement of primary and secondary basins in our AOI. The popularity of determining primary minibasins has risen from the improvement of the depth imaging of these basins (Pilcher et al., 2011). Specifically in the Gulf of Mexico where the Miocene strata deposited around the salt canopy can become incased in the salt creating secondary incased minibasins. The Miocene strata that can be found in these minibasins is one of the primary targets when prospecting for oil and gas in the GOMB. Proficiencies in

imaging below a salt canopy have allowed for the primary minibasin to be better imaged, therefore mapping of poorly lit, seismically transparent areas can be carried out using basic seismic stratigraphic methods to interpret the surrounding strata, determining the location of the salt feeder to then map the surrounding strata (Pilcher et al., 2011).

3.2 Megaflap

Megaflaps are defined as basin edges thinning towards the diapiric walls bounding the minibasin. The sediment layers are folded and overturned as evaporite extrusion occurs at the surface and “flapped” onto the basin center (Figure 6). These thick sediment layers thin upward as they are upturned (Jackson and Hudec, 2017). Megaflaps are intricately linked to diapir initiation. Once the salt has been mobilized, the strata located above the salt that was once continuous, become pierced and uplifted as the salt moves upward (Nikolinakou et al., 2017). Megaflaps are vital to understanding diapir evolution properly. The main factor in megaflap development is the rate at which salt becomes allochthonous or allochthony. This mechanism occurs when local salt extrusion is quicker than the sedimentation rate (Jean et al., 2016). Megaflaps are found in deep-water fold and thrust belts on passive margins in the northern Gulf of Mexico (Rowan and Ratliff, 2012).

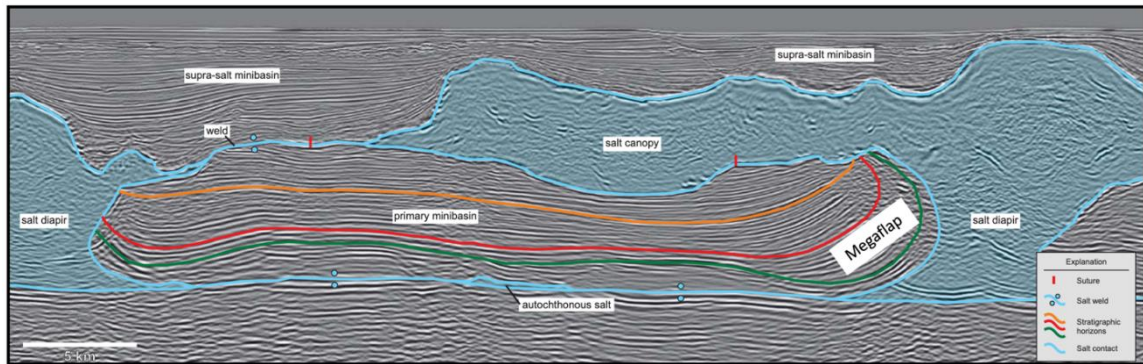


Figure 6. 3D post stacked depth migrated seismic line from the northern Gulf of Mexico illustrates the location of primary and secondary (supra-salt) minibasins, salt welds and expulsion rollover. Seismic unit overturning and thinning towards the base of the salt canopy creates a megaflap. Modified from Hearon et al. (2013).

3.3 Salt Feeder

The recognition of salt feeders and proper interpretation of the location and orientation of the salt a crucial to understanding canopy evolution. The correct placement of the salt feeder is extremely important when prospecting around the salt stock canopy. Interpreters can be tempted to drill the structural highs that are usually overly the salt feeder. Incorrect placement of the feeder can result in drilling directly through the feeder's axis (Jackson and Hudec, 2017). Traps form along the flanks of the feeder and are a common target when prospecting around salt stock canopies. Interpretations must be done using a 3D seismic set. Salt stocks and feeders in a single 2D line may appear to be two distinct separate salt bodies one overlying the other separated by strata, while in fact, the lowermost of the salt could be the base or pedestal of the salt.

More specifically flanks of salt feeders have dips around 90° (Mattson, 2019), and horizon mapping tools in seismic interpretation software reach their limits in beds dipping around 70° . Mapping horizons is based on picking X (spatial point), and Y (depth/time value) pairs that can then be connected and then later used to create grids and maps. The steep flanks will result in more than one spatial point per depth value that most of the current-day software cannot handle

3.4 Salt Welds

During halokinesis, the mobilization of salt results in zones or surfaces where the strata that were originally separated by salt, encounter one another as the salt was removed. The result is a salt weld, where the surface or thin zone marks a vanished salt body (Jackson and Hudec, 2017; Hudec et al., 2011). Salt welds have numerous classifications based on the thickness of the salt left in between areas adjoining strata. Salt welds are also classified by the geometry of the salt before welding has occurred (Jackson and Cramez, 1989; Jackson and Hudec 2017). The recognition and classification of salt welds are important for two main reasons. First, the salt weld can act as a seal or migration pathway during hydrocarbon generation.

4.TECTONIC FRAMEWORK

The Gulf of Mexico is a small ocean basin located between the North American plate and the Yucatan block that is characterized by extensional rift tectonics and wrench faulting (Galloway, 2008; Mancini et al., 2001). The basin has undergone numerous long-term tectonic evolutions and short-term eustatic changes along with climatic-influenced sedimentation, evolving as a passive margin from the counterclockwise rotation of the two plates (Hudec et al., 2013; Hearon, 2013). These events can be summarized in three phases that occurred during the Mesozoic, 1) Post – Orogenic Successor Basin Fill and Rifting Phase 2) Middle Mesozoic Drift and Cooling Phase 3) Late Mesozoic Local Tectonic and Crustal Heating Phase (Snedden and Galloway, 2019).

The first phase of active rifting occurred from the Late Triassic – Early Jurassic (210 – 163 Ma) (Ewing and Galloway, 2019; Jackson et al., 2013). This rifting is the initiation of the breakup of Pangea, where the Yucatan plate moved southeast, coupled with South America rifting from Yucatan and seafloor spreading. The spreading of the plates allowed for the deposition of the Eagle Mills Formation. It is characterized by graben formation throughout the periphery of the basin, filling with redbeds and volcanic rocks (Hudec et al., 2013). Crustal attenuation and the formation of transitional crust occurred throughout the region at this time.

Phase 2 occurred during the Middle Jurassic through the Early Cretaceous. During this time, the North American plate continued to separate from the Yucatan Block, further creating a defined limit of the basin as the transition from active rifting to a passive margin was occurring. The separation of the plates created new faulting systems and deepened pre-existing rifts and grabens (Galloway, 2008). The extensive evaporite known as the Louann Salt began filling the newly formed grabens and minibasins throughout the Gulf of Mexico (Jackson et al., 2013) (Figures 7 and 8). The exact age of the salt is not known but is generally agreed to be Callovian in age (Snedden et al., 2018). There is continual debate on whether seafloor spreading occurred prior to the deposition of the Louann or if seafloor spreading commenced near the end of the Louann deposition. Hudec et al. (2013) believes sea floor spreading started well after the deposition of salt. However definite evidence is absent on when the spreading occurred since the estimates are all based on plate reconstruction models or the assumption that the salt terminated where the sea floor spreading commenced (Hudec et al., 2013)

Phase 3 occurred during the Early Cretaceous through the Cenozoic (Ewing and Galloway, 2019; Snedden and Galloway, 2019), consisting of continual subsidence along the tectonic hinge zone of thick and thin transitional crust (Méndez-Hernández, 2008). It consisted of seafloor spreading that led to the formation of oceanic crust in the deep central area of the GOMB. During this phase the continual subsidence of the basin allowed for the large accumulation of sediment to be deposited. As result of the previous phases of crustal stretching, 5-7 km of subsidence occurred (Galloway, 2008) creating

new accommodation space for sediment deposition. The warm shallow marine condition during the Early Cretaceous led to large limestone deposits on the basin margins created the modern outline of the GOMB (Gulf of Mexico basin) (Galloway, 2008, Snedden and Galloway, 2019). The deeper areas of the basin were dominated by clastic sedimentation from large river systems. The fluvial systems created large deltaic deposits along with turbidity and debris flows that fill the secondary minibasins discussed later. The accumulation of the sediment was the main driving mechanism for the movement of the Louann Salt and resulted in various salt related structures across the basin. The deposition of thick sedimentary packages alongside the structural traps created by the salt tectonics has created on the world's most prolific hydrocarbon provinces (Snedden and Galloway, 2019).

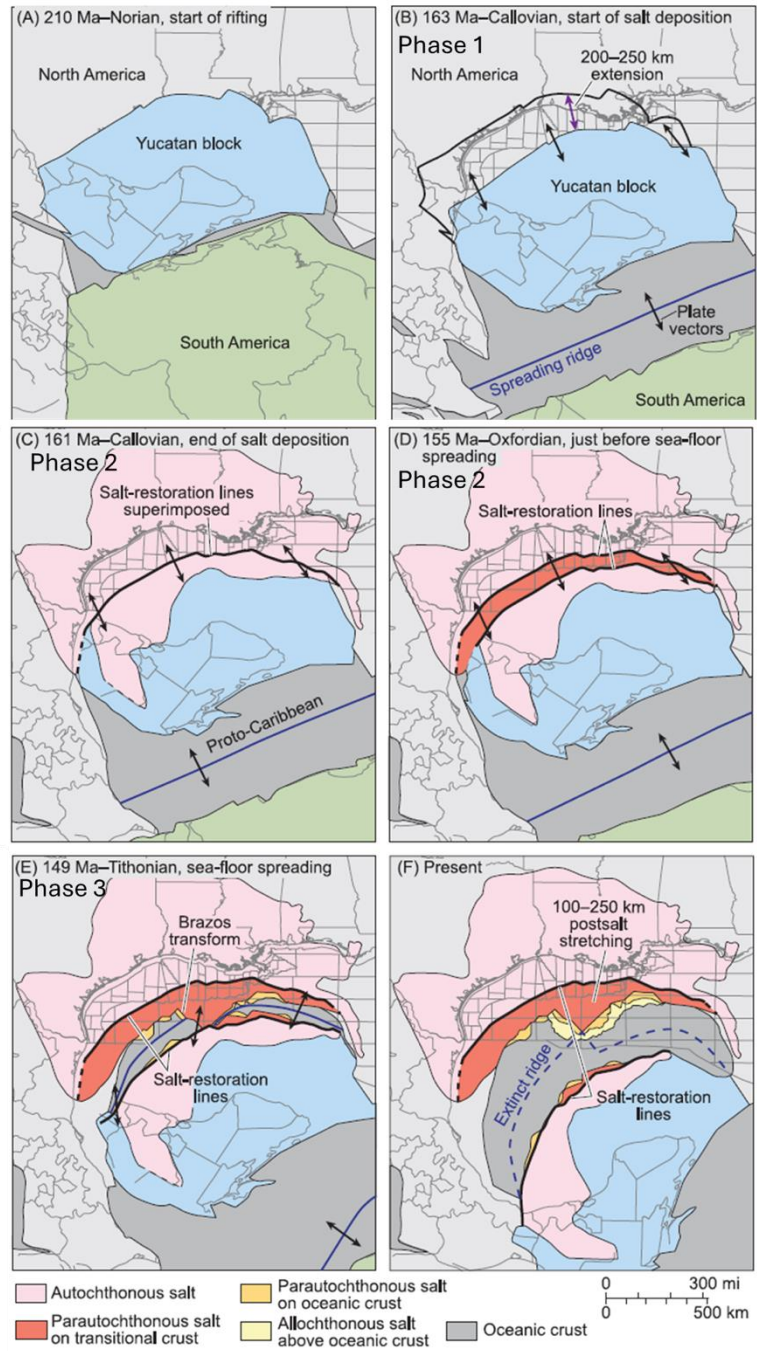


Figure 7. Plate reconfiguration and salt deposition during the GOMB formation throughout the Late Triassic to modern day. Modified from Jackson et al. (2013).

5.STRATIGRAPHY

The basement of the GOM is deformed Paleozoic rocks that outcrop north beyond the boundaries of the Appalachian and Ouachita orogenic belt (Wu et al., 1990). The stratigraphy beneath the salt is not well known and is believed to be syn-rift continental clastics that occur above the rifted basement (Fiduk, 1999). Overlying the salt, the observed sequence of shallow marine carbonates changes upwards into deep marine carbonates and shales, indicating rapid subsidence of the basin (Fiduk, 1999) (Figure 8 and 9).

The continental slope of the GOM has been heavily influenced by the Louann Salt halokinesis. Early work on the Louann Salt suggested that the complete salt masses associated with the Sigsbee Escarpment were allochthonous. This was suggested by cross sections of the northern GOM where the extensive listric normal faults dissect the Tertiary clastics (Wu et al., 1990) Gravity-driven deformation has resulted in salt rollers that have developed salt tongues and sheets on the continental slope of the GOM. The allochthonous salt body in our section is surrounded by Miocene-aged sediments that are overlaid by newer Pliocene layers. The end of the GOMB spreading occurred during the Early Cretaceous and marked the beginning of the six composite depositional episodes in the northern GOMB (Galloway et al., 2000). The Cenozoic interval is a thick siliciclastic

package of sediment further divided by fossiliferous marine shale tongues that recorded regional transgressions across the northern basin.

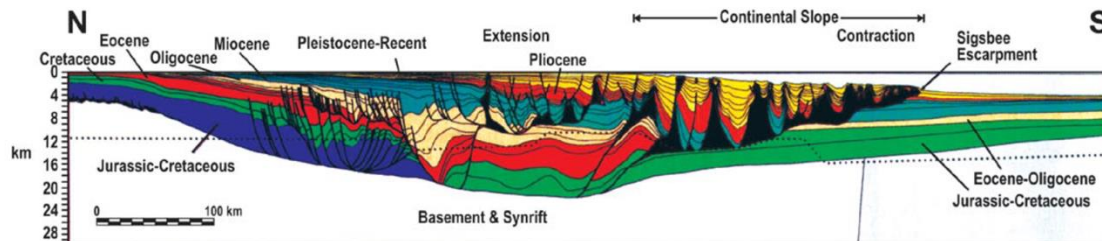


Figure 8. General North-South cross section of the Gulf of Mexico and its complex relation between the salt (black) and intraslope sediments. Modified from Fisher et al. (2007).

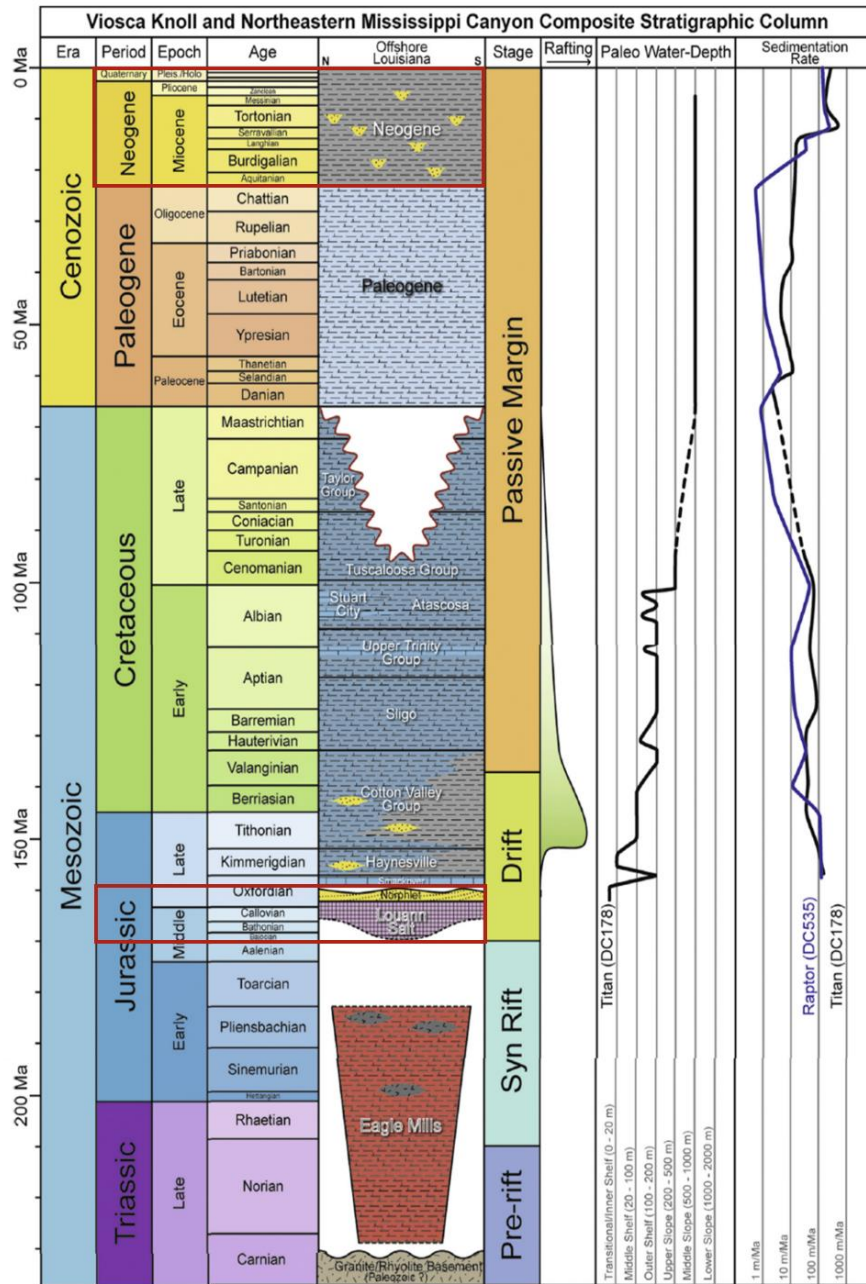


Figure 9. Stratigraphic column of the northeastern Gulf of Mexico. Formations of interest are outlined in red. Modified from Mattson et al. (2020).

5.1 Louann Salt

The Louann Salt is a massive bed consisting largely of silty, sandy massive halite with intercalated anhydrite (Mancini et al., 1990). The Louann Salt has been assigned ages from the late Bathonian to early Oxfordian based on its stratigraphic relationship with adjacent units (Mancini et al., 1990). Primary deposition of the Louann Salt was conformably over the Werner Formation, or where the Werner is absent, it disconformably overlies the Eagle Mills or basement rocks (Erlich et al., 2022; Mancini et al., 1990). The deposition of the Louann Salt coincides with the initial phases of seafloor spreading and is considered to be the first basin-wide depositional unit with thicknesses ranging up to 6,000 feet (about 1.83 km) in some regions of the basin (Galloway, 2008; Mancini et al., 1990). Thus, the accumulation of the Louann was distributed across the thinned transitional crust that was then later transported basinward towards the continental slope. The discovery of two Jurassic-aged salt bodies in the GOMB gave for the idea that the two salt bodies were once linked together and then later separated by the seafloor spreading. In the northern GOMB we find the Louann Salt (Snedden and Galloway, 2019). The southern counterpart is called the Isthmian salt and is found in the Campeche and Yucatan salt basins (Hudec et al., 2013).

5.2 Norphlet Formation

The deposition of the Norphlet Formation occurred during the Late Jurassic in an arid continental setting. The Norphlet Formation overlies the Louann Salt and underlies the Smackover Formation. The Norphlet Formation consists of a thin bed of a

discontinuous basal black shale followed by a thicker bed of arkose sand, and trace amounts of hematite are also found in some locations (Mancini et al., 1985). The lower beds of arkose change to frosted grains in the upper beds that form aeolian dunes (Hunt, 2013). The boundary between the Louann and the Norphlet is poorly defined but a sharp contact with the overlying Smackover formation exists. The Norphlet Formation is mostly located in the northern and northwestern Gulf margin (Galloway, 2008; Hunt, 2013).

5.3 Miocene – Pliocene

The Miocene-Pliocene sedimentation that occurred in the northern Gulf of Mexico consists of nearly 23 million years of coastal deltaic and shore-zone deposition (Galloway, 2001). Regional studies have described the deposition as highly aggradation to progradational shore zone successions that are hundreds to thousands of meters thick (Galloway, 2001). The long-term changes in rate and location of sediment supply define three episodes within the Miocene.

The Miocene basin fill is divided into three depositional episodes that cover millions of years and record the deposition of the gulf transitioning from the northwestern to eastern margins. The initial episode of deposition is the basal Miocene Oakville Formation, followed by the Fleming Formation and eventually the middle Miocene Goliad Formation. The lower Miocene was dominated by high rates of sedimentation supply and continental margin outbuilding followed by a defining break of approximately

18 million years where a transgressive stage divides the lower portions of the lower Miocene (Galloway, 2001).

The middle Miocene was a shorter interval that introduced sediment sourced from the paleo-Mississippi and paleo-Tennessee rivers where the dominant sediment input advanced the continental margin to as much as 70 km (Galloway, 2001). The upper Miocene was a longer 6-million-year interval that was dominated by sediment input from the paleo-Mississippi and paleo-Tennessee much like the middle Miocene. During this episode, as much as 5 km of sediment was deposited in the east-central Gulf and across the basin margin. The sediment loading continued to rework the salt basinward (Galloway, 2001).

Depositional patterns in the Pliocene record the climate changes affecting the North American continent along with global glacioeustatic sea level changes. The creation of a singular large river drained into the central GOMB created widespread delta and advanced slope apron systems. Minibasins in this area continue to be filled by delta-fed turbidites, channel/lobe complexes, and debris flows by a continual Quaternary Mississippi fan system. Overall, these sedimentary packages are largely deformed by the salt diapir in the region, allowing for Jurassic-aged evaporites to lie directly above or below the younger Miocene-Pliocene sedimentary units.

5.4 Mobile Shale

The location of the shale unit located above the salt is dispersed throughout our survey area (Figure 10). The mobile shale layer is located within the Miocene intervals; a specific age for shale was not obtained. Mobile shales are commonly found as surficial mud volcanoes, shale-cored folds, and deeply buried shale diapirs. Exploration around these mobile shales is both difficult and challenging. Mobile shales in our AOI follow the definition by Soto et al., (2021) where they are bodies of clay-rich sediment or sedimentary rock undergoing penetrative, (visco-) plastic deformation at the critical state (Soto et al., 2021). The mobility of shales is believed to arise from the over-pressured state that simply caused the shale to become mobile. During the overpressure state the shale goes through particle dissolution, grain rotation and sliding, pore reduction and the expulsion of the clay bound water in the pores (Soto et al., 2021). Shales then stop moving when the shear stress drops below the critical state (Soto et al., 2020

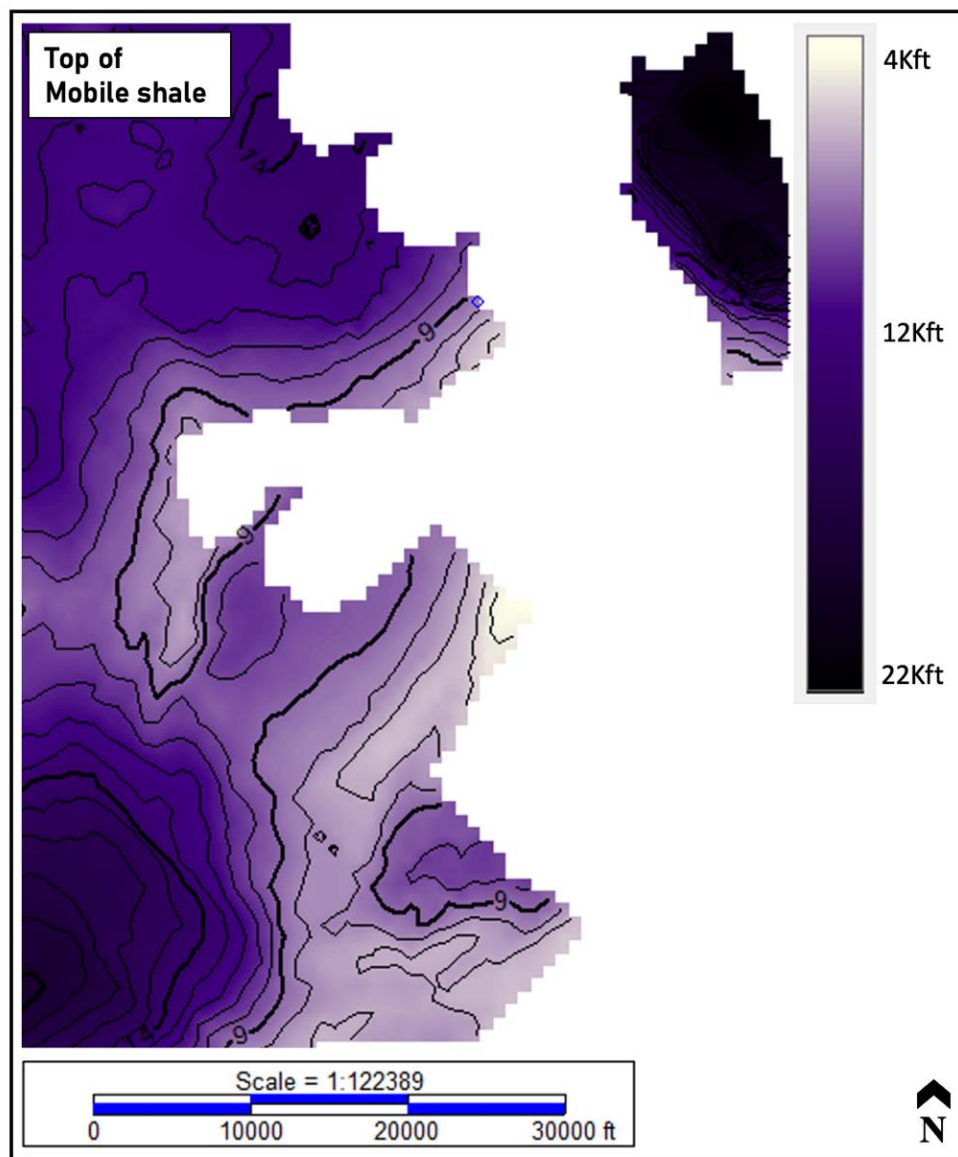


Figure 10. Depth map to the top of the Mobile shale created in Kingdom Suite.

6. METHODS

The materials used to complete the project are publicly available reports of the Gulf of Mexico over our area of interest, public well log data, and proprietary seismic data. Interpretation of the salt structure of surrounding strata was accomplished using a 3D seismic data set. Seismic data was obtained from WesternGeco using their proprietary processing software to produce the multiclient EDGE survey (Figure 11). The location of the seismic data set being used is in the Green Canyon protraction of the GOMB located on the outer limits of the continental shelf north of the Sigsbee Escarpment (Weiland, 2008). The Puma West GC821-002 well is located in this area, and well log data is publicly available through the Bureau of Ocean Energy Management.

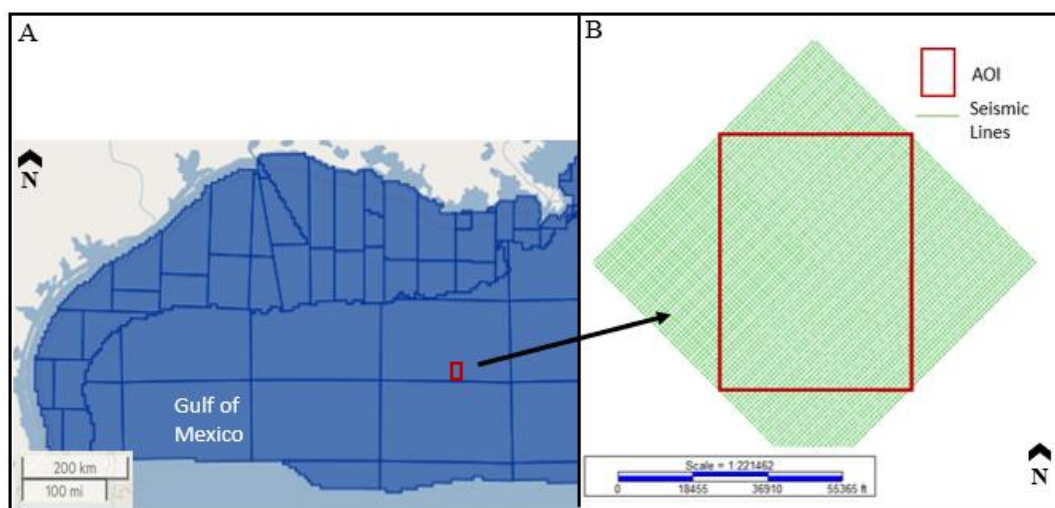


Figure 11. (A) Gulf of Mexico Basin with protractions outlined in blue showing the area of interest (AOI) and (B) a close up of the AOI with the 3D seismic grid.

The survey is a multiclient 3D depth survey that combines both wide azimuth acquisition (WAZ) and full azimuth acquisition (FAZ) datasets (Table 1) to produce a final image. FAZ acquisition uses a combination of WAZ and Multi azimuth. The use of more azimuths allows for improved illumination and resolution by having a higher fold count to enhance the signal-to-noise ratio (Hung and Yin, 2012). The final depth migrated volume was used for interpretation in this study. The seismic volume has an inline/crossline spacing of 25 m with a sampling rate of 9.7 m. The full stack volume was processed at zero phase representing American polarity. The improvements in the acquisition, pre-processing, pre-stack, and post-stack seismic methods have improved the accuracy of imaging around and through large evaporite bodies.

Using seismic sequence stratigraphic techniques, a series of horizons were mapped throughout the section using Kingdom software by S&P Global (formally IHS), specifically the top and base of the allochthonous salt and the parautochthonous salt located in the AOI. To increase the validity of the markers picked, the incorporation of the GC821-1 well was used. The geophysical information from the well was introduced into our seismic interpretation software to allow formation tops to be picked by creating synthetic seismograms that allow for precise formation top interpretation through the section. The allochthonous and parautochthonous salt found in our study area were carefully mapped. The base and top of strata of interest were then gridded, which was then used to produce isochron and isopach maps. These grids were used as a visual aid in accessing the structural framework of the salt dome (Figure 12). The interpretation of the

salt was picked on the final depth volume picked on a base of salt where the salt velocity assigned was used. The capability of the Kingdom software allowed for 3D visualization of the dataset for interpretation.

The creation of a synthetic seismogram is essential to help bridge the gap between time, the raw measurement of subsurface data, and depth, the most common way of expressing subsurface distance. The creation of the synthetic is carried out using the Kingdom software that requires a few key items: a velocity curve, obtained from the raw petrophysical data of the Puma well; a T-D chart, obtained through publicly available publications; and a wavelet that the software lets the user determine. For the synthetic created, the Ormsby wavelet was used.

A thorough analysis of the post-stack time migrated 3D seismic section commenced on the southwestern end of the data and progressed through the northeastern end. The stratigraphic seismic units that surround the high have an increased signal-to-noise ratio allowing for finer scale details to be seen.

The mapped seismic horizons were selected based on their high-amplitude response; lateral continuity that bound seismic-stratigraphically important packages that define specific tectono-sedimentary phases of minibasin development. Seismic attributes (i.e. variance and chaos) were used, generated along or between these horizons, to identify deep-water depositional elements. Variance and chaos attributes image spatial discontinuities in seismic reflection events, which could relate to important structural

(e.g. intra-MTC or Mass Transport Complexes) and or stratigraphic discontinuities (e.g. the abrupt seismic facies change from seismically chaotic MTCs to more continuous slope strata). (Wu et al., 2020).

Table 1. Acquisition parameters for EDGE survey (Courtesy of WesternGeco).

Acquisition Parameters – WAZ		Acquisition Parameters – FAZ	
Recording system	Q-Marine* point-receiver marine seismic system	Recording system	Q-Marine* point-receiver marine seismic system
Energy source	Single source: 8,475 in ³	Acquisition configuration	Dual Coil Shooting* multivessel full-azimuth acquisition
Source depth	10 m	Energy source	8,475 in ³
Streamer configuration	Multistreamer: ten 7,000 m cables to ten 8,000 m cables	Source depth	10 m
Streamer depth	12 m	Streamer configuration	Multistreamer: ten 8,000 m cables
Maximum offset	8,600 m to 9,600 m	Streamer depth	12 m
Sample rate	2 ms	Maximum offset	14,000 m
Record length	14 s	Sample rate	2 ms
Digital group forming (DGF) receiver interval	12.5 m	Record length	16s
Recorded bin dimensions	6.25 × 60 m	Digital group forming (DGF) receiver interval	12.5 m
Acquisition completed	December 2006 to April 2011	Acquisition completed	March 2012 to February 2014

Interpretation of a total of 7 horizons were mapped in our area. Interpretation commences directly above the autochthonous salt; the reflection below the autochthonous salt is interpreted to be basement rock that exhibits poor continuity and no layering. The 7 horizons mapped were picked based on petrophysical data, seismic reflectivity and correspond to the horizons mapped by Pilcher et al. (2011); Bui et al. (2011); and Moore (2013). Horizons correlate to the deposition of Cretaceous aged strata through Recent – Pleistocene strata.

Often, minibasins are filled with mass transport deposits. Mass transport deposits (MTDs) are composed of deposits from slides, slumps, and debris flows. The MTDs are found in a wide range of water depths and slopes from 0.5-10° (Sawyer et al., 2009). The

dark continuous reflectors mapped in secondary minibasins across the diapir are condensed sections that are presumed to have widespread deposition during high Pleistocene Sea level. Mass Transport Complexes (MTCs) are defined as a seismic stratigraphic term that can only be applied to features that can be seen at scale on volumetrically large seismic surveys (Weimer and Shipp, 2004). Thickness can range from 5 – 100's of meters where the top surface is found to be commonly errored while the base surface can be planar, erosional to stair stepped (Weimer and Shipp, 2004).

Seismic facies are distinct seismic reflection patterns that represent different lithologies, depositional environments, or structural features (Snedden and Galloway, 2019). The seismic facies are identified by features such as the continuity, frequency, direction, and strength of amplitude reflection (Snedden and Galloway, 2019). Continuity and strength of amplitude reflection were used to help match well defined seismic facies boundaries to the defined time periods that were then used to map the horizons shown in

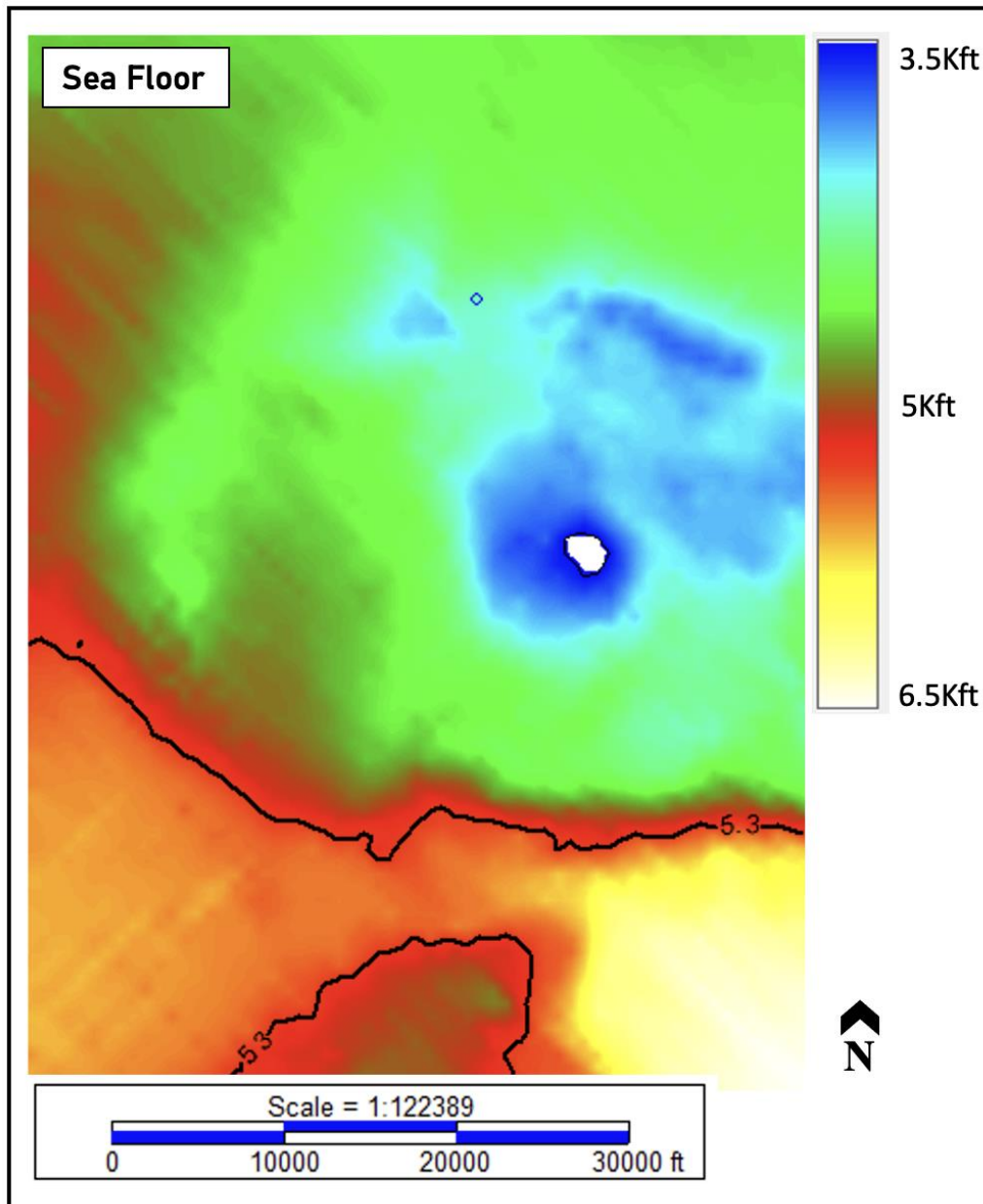


Figure 12. Grid of seafloor reflector from 3D post migrated data Kft from sea level.

7. RESULTS

The Puma Diapir area is a salt feeder connected to a shallow canopy. The diapir is on the southeastern edge of the Sigsbee Escarpment in the deep water of the GOM. Overall, the strata above the salt canopy are dominated by normal faulting patterns due to the extension and movement of salt. No faults were seen under the salt canopy. While faulting can occur and may be present, the absence of faulting under the canopy could be due to the diminishing resolution of the seismic. The extensional faulting mapped is concentrated above the shallowest point of the canopy, noting the current passive stage of diapirism; the enhanced resolution of the seismic enables detailed mapping of the faulting to be achieved. Normal faults in the AOI originate from the ridges found on the edges of the minibasins depressions mapped. The interplay of sedimentation and salt rise resulted in various salt structures above the salt canopy. The most noticeable of these being the minibasins. A total of five secondary minibasins are in the AOI and formed from salt withdraw. This section will go into details on individual features observed in the AOI.

7.1 Horizons

Finding and determining the seismic horizons that will be used across the survey is a necessary step to properly structurally analyze an area. Using a seismic interpretation software, mapping of seismic reflection are traced throughout the survey. Identifying the reflections are typically based on the amplitude, phase morphology and continuity that

change because of differing lithology. (Yang and Sun, 2020). Mapping of the horizons begins directly above the base autochthonous salt. A large feature of low reflectivity is observed throughout the section that is interpreted to be a large allochthonous salt body, above we find numerous faults with increased seismic reflectivity. The top of the salt body in the shallowest parts is extremely close to piercing through the seafloor. This structural high is prominent when looking at seafloor bathymetry maps.

A total of seven interpreted horizons were mapped in our area (Figure 13). Picking commences directly above the autochthonous salt; the reflection below the autochthonous salt is interpreted to be basement rock that exhibits poor continuity and no layering. The seven horizons mapped were picked based on petrophysical data, and seismic reflectivity and correspond to the horizons mapped by Bui et al. (2011); Pilcher et al (2011); and Moore (2013). Horizons correlate to the deposition of Cretaceous – aged strata through Pleistocene – Recent strata.

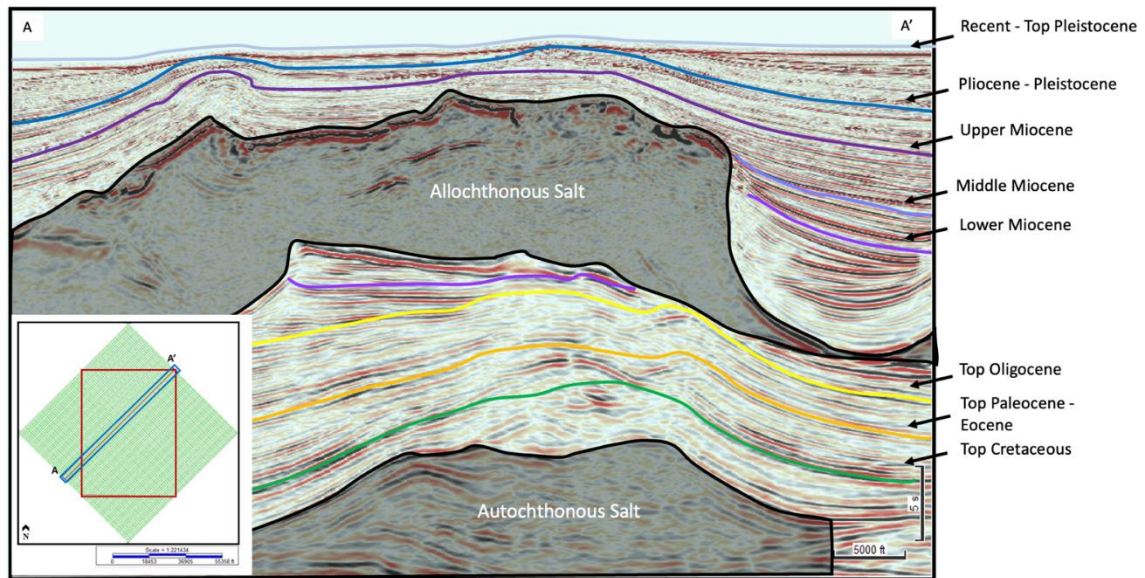


Figure 13. Inline 6541. The lower shaded grey is the autochthonous salt, upper is the salt canopy. Horizons mapped throughout the data set. Top Cretaceous (T1), Top Paleocene – Eocene (T2), Top Oligocene (T3), Lower Miocene (T4), Middle Miocene, Upper Miocene (T5), Recent – Top Pleistocene (T6).

7.2 Minibasins

Five secondary minibasins are found at the Puma Diapir (Figure 14 and 15).

These secondary minibasins are above the allochthonous salt canopy found predominantly on the western side of our data set. There is one primary minibasin located under the salt canopy.

Seismic facies were picked from analogue (Arfai et al., 2016; Campbell, 2005; Martinez et al., 2024; Omosanya and Harishidayat, 2019) information provided by seismic re-flection and well-based analysis of similar depositional systems in adjacent area by Wu et al. (2020). Secondary minibasins are dominated by two seismic facies. The layered units are composed of interbedded layers of shale and sandstone; these appear in

the seismic sections as being bound by a highly reflective seismic curve response that parallels the bounded strata at the base and tops of the surfaces. Within the seismic units, the strata are characterized by parallel surfaces with medium to low amplitude reflections. The depositional environments of these layered units are inferred to be levees, lobes, and channel systems. The second seismic facies that infills the secondary minibasins are Mass-transport complexes (MTCs), deposits of subaqueous mass flows, and comprise slides, slumps, and debris-flows (Dott, 1963; Nardin et al., 1979; Posamentier and Kolla, 2003). These appear in the seismic data as discontinuous strata that is faulted and folded with low to medium amplitude seismic reflectivity, often with chaotic internal reflection patterns. This chaotic seismic series records the related process creating the MTC, such as slumps, slides, and debris flows. The identification of the seismic facies helps define depositional environments and different lithological packages, and highlights the structural features found within the minibasins. Seismic units were picked using the facies discussed above and are numbered starting with number one for the lowermost unit in the minibasin and continuing numbering towards the seafloor.

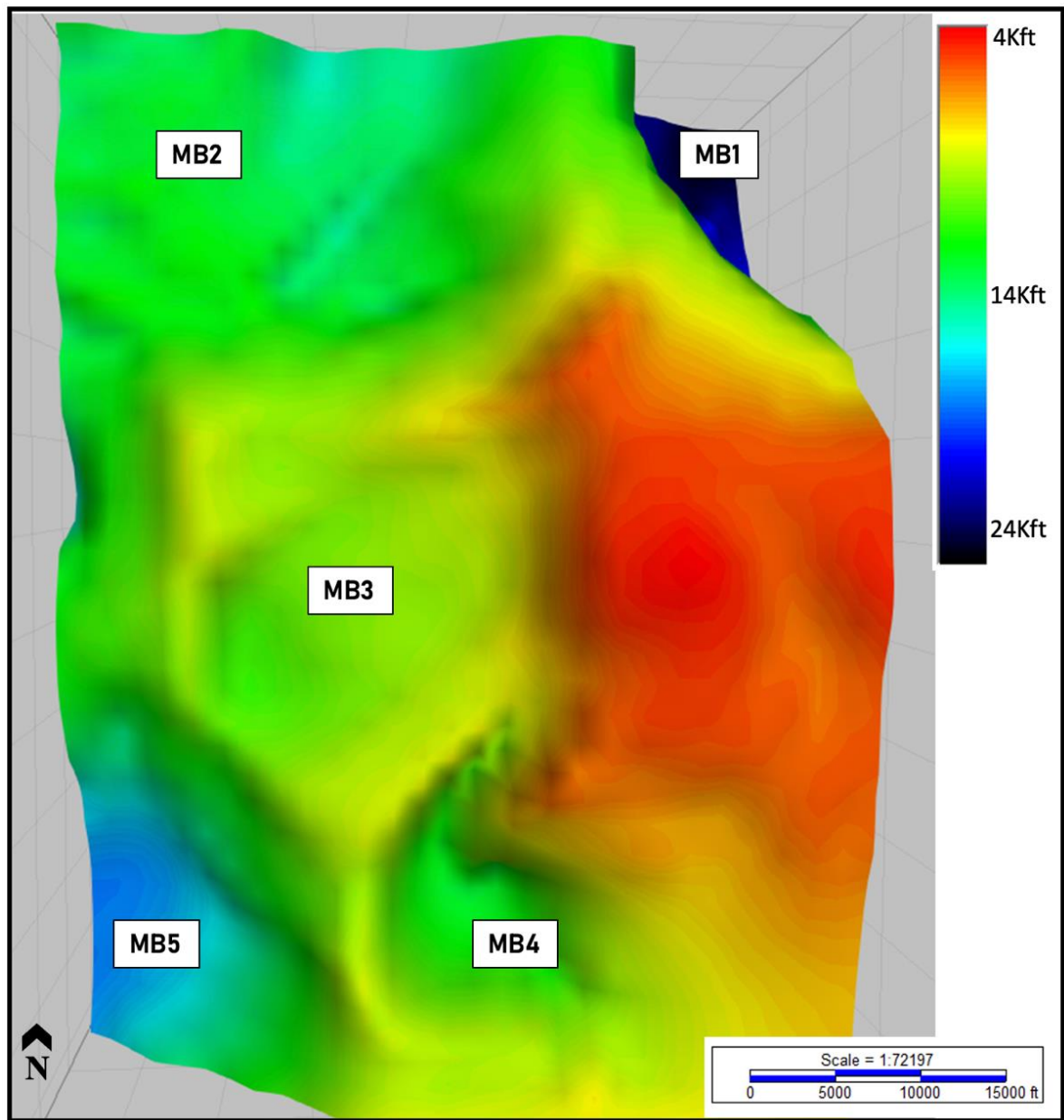


Figure 14. Depth map (depth below sea level in Kft) for top salt, showing the overall salt-tectonic structure of the study area with the impression of the five secondary minibasins on the top of the salt canopy. The location of the primary minibasin (MB6) is not shown.

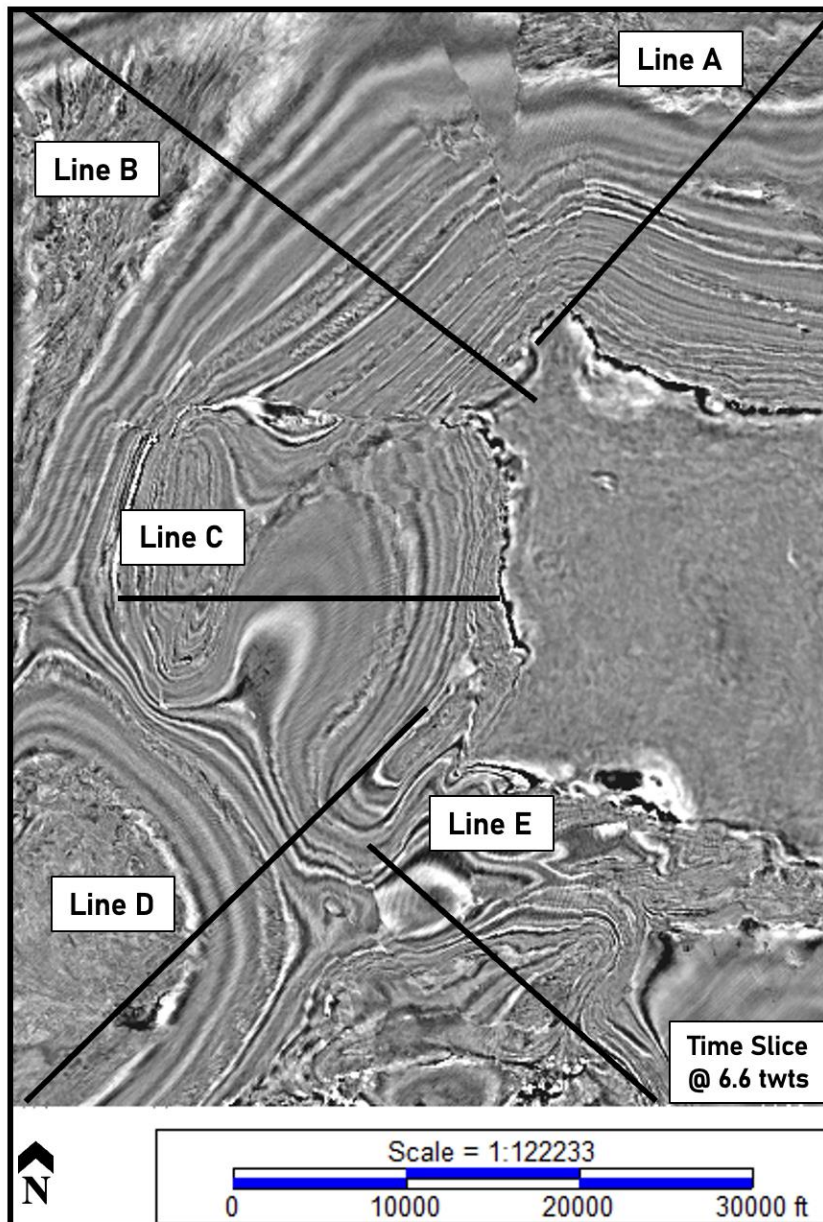


Figure 15. Time slice of data @ 6.6 [twts] truncation the secondary minibasin. Location of seismic lines used in seismic unit horizons. Line A ((Figure 15), minibasin 1), Line B ((Figure 16), minibasin 2), Line C ((Figure 17), minibasin 3.), Line D ((Figure 18), minibasin 4), Line E ((Figure 29), minibasin 5).

7.2.1 Minibasin 1

Minibasin 1 is a secondary minibasin, where the deposition of sediments has created a bowl shaped minibasin with a welded base (Figure 16). The diameter of the basin visible in the data set is approximately 6.9 km across measured from the southwest to the northeast where the sediment onlaps against the salt. The top of the basin is at 4.46 Kft, the base is at 25.28 Kft. The basin is filled at the base by upper Miocene sediment overlaid by Pleistocene strata. The southern side of the minibasin has an onlapping margin where the upper Miocene strata thin out against the edge of the salt. This lateral change in the upper Miocene units shows syn deposition of the units, where the salt rise rate was higher than the depositional rate. This allows for increased sedimentation towards the center of the units and a thin edge that onlaps the salt diapir. The minibasin is bowl shaped from the observed section. A total of 18 seismic units (SU) are in minibasin1. SU1 is located directly above the welded base of the basin. SU10 is the top unit of the Upper Miocene, overlaid by Pliocene sediments. The units are interbedded layer of sand and shale. The reflections of the sand and shale are continuous and predictable. The reflections of the MTCs do not follow the same reflection pattern of the

sand shale, as the MTC are chaotic and discontinuous. Three MTCs are found in shallow Pleistocene strata from 5 Kft to 10 Kft.

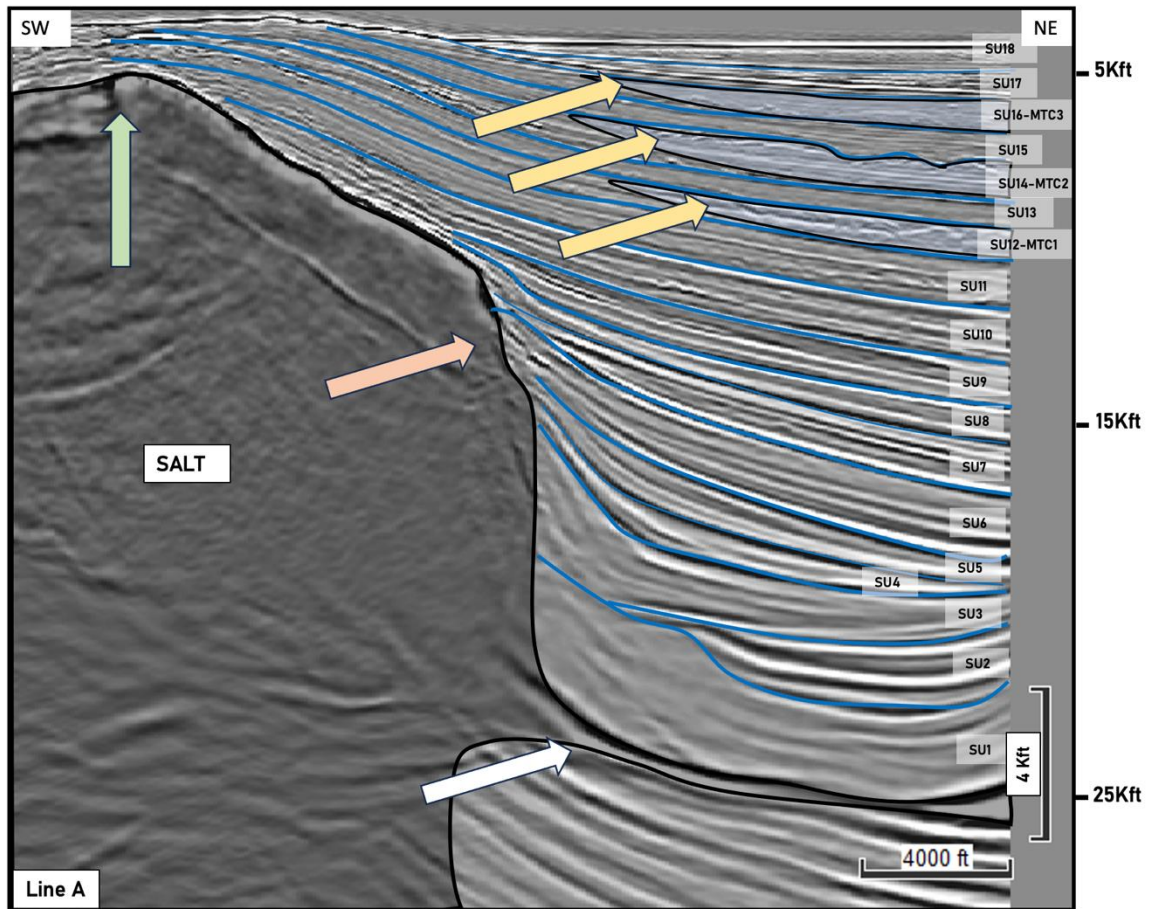


Figure 16. Seismic section of minibasin 1. Location of this line (Line A) is shown in Figure 15. Minibasin 1 consists of a bowl shaped minibasin with a welded base. (white arrow), draping of strata against the salt (orange arrow), and thinning of overlying strata (green arrow). The 3 MTC found are shaded and outlined (yellow arrows).

7.2.2 Minibasin 2

Minibasin 2 is a secondary minibasin, approximately 10.9 km across in diameter (Figure 17). The elongated basin axis trends NE – SW and deepens towards the NE. The basin rests atop the salt canopy. A total of 11 seismic units composed of interbedded

layers of sand and shale are widespread and are continuous across the minibasin. Four MTCs are in the minibasin and nearly span the entirety of the area. The MTCs are prominent and can easily be distinguished from the other reflections found (MTC 1 – MTC 4). SU1 is the lowermost unit that is composed of the mobile shale seen across the top of the salt canopy. There is a small amount of mobile shale in SU1 that overlies the chaotic surface of the top of the salt. The pits along the top of the salt are thought to result from the interaction between the mobile shale and the evaporite body. Areas that show diminished mobile shale correlate to the pits seen in this area. Seismic units 2-4 overly the mobile shale and are continuous with a minimal number of reflectors seen in between the bounding surfaces. SU1-3 span the entire minibasin as they thin towards the salt dome that is nearing the seafloor. SU4- SU11 were deposited as the salt withdrawal deepened the minibasin, as indicated by the SUs thinning toward the edges of the basin and thickens at the center.

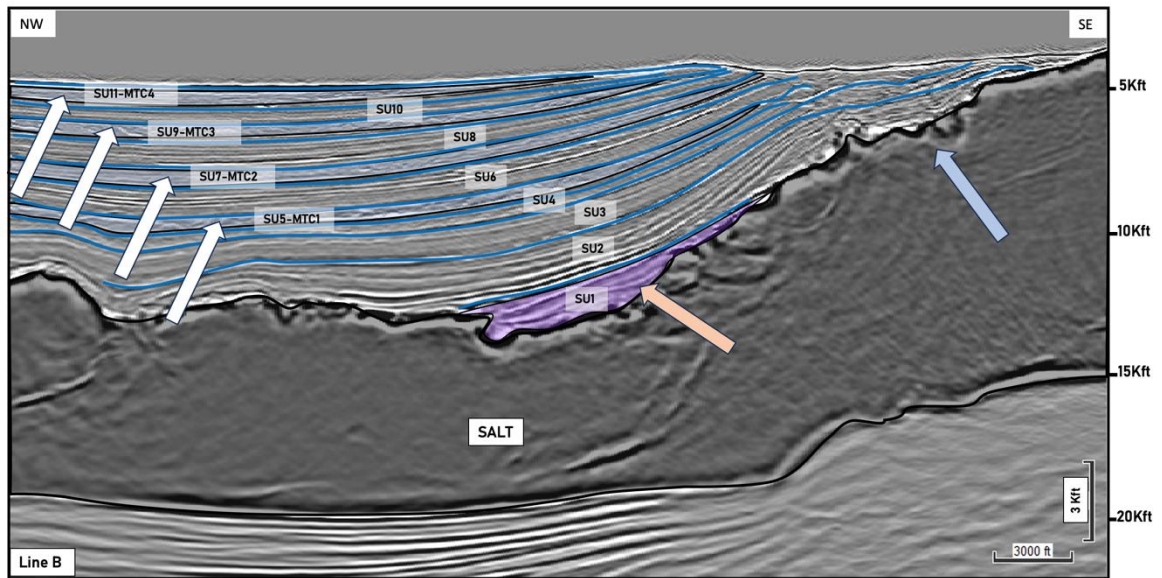


Figure 17. Seismic section of minibasin 2. Location of this line (Line B) shown in Figure 15. The elongated basin has four MTC that thin towards the salt high. (white arrows), localized zone of mobile shale (orange arrow), chaotic top of salt with no visible mobile shale (blue arrow).

7.2.3 Minibasin 3

Minibasin 3 is a secondary minibasin, approximately 6.1 km across in diameter (Figure 18). Minibasin 3 is the smallest and shallowest of the secondary minibasins. It measures approximately 6.1km across and is approximately 11 Kft to the base. The minibasin is an elongated oval shape. A total of eight SUs were distinguished in the minibasin. SU3 – SU8 had the same continuous reflection properties where the internal layering of the seismic units follows the bounding surfaces. SU1 does not have a layered internal reflection, instead, it is seismically transparent and is interpreted to be the mobile shale unit found in the AOI. The top surface of the minibasin is slightly pitted. It is noted that in the areas where less mobile shale is found the surface is more chaotic and more

seismic reflection surfaces are seen inside the large salt canopy. SU2 is partially seismic transparent but has internal reflectors matching the seismic facies of the MTC found in minibasin 1,2 and 5. Seismic units in the section thin towards the structural highs of the salt canopy created by salt withdrawal. As the sediment was being deposited, the salt was moved outward and up towards the surface.

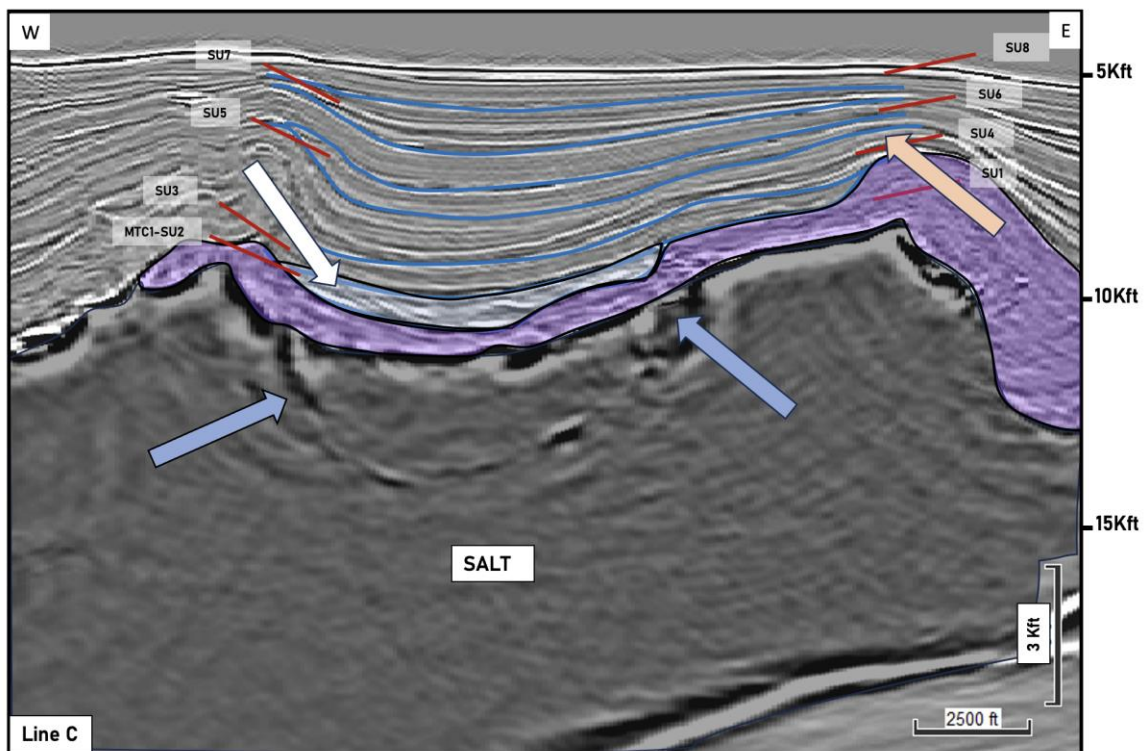


Figure 18. Seismic section of minibasin 3. Location of this line (Line C) is shown in Figure 15. One MTC found in the lower units of the basin. (white arrow pointing to shaded area of MTC unit). Areas of rough salt surface located under the mobile shale with increased internal seismic reflectors (blue arrows), seismic units displaying syn depositional shape as they thin over the salt high (yellow arrow).

7.2.4 Minibasin 4

Minibasin 4 is a secondary minibasin, approximately 7.7 km across in diameter located on the southern edge of the salt canopy where the salt is being thrust towards the sea floor (Figure 19). The base of the basin is at approximately 14 Kft. The edge of the basin terminates, at the tip of the salt where SU1 has been upturned towards the sea floor. The near horizontal dip of the SU1 has created a bowl shaped minibasin where the other units thin and onlap the structural high created by the roof edge thrust. It is composed of six seismic units; the basal unit in the basin encompasses the largest accumulation of mobile shale measuring approximately five Kft in thickness. Mobile shales are commonly found in settings alongside salt bodies because they both are weak ductile materials that form diapirs (Hudec et al., 2023). The criteria needed for the development of mobile shale is a thick salt sequence and a thick rapidly deposited mud prone section, both conditions are met in the GOMB and visible in our AOI. Here we find the detachment of the Eocene-Oligocene salt. The shortening events of the Oligocene-Miocene overlap result in thrusting resulting in folding cored by the mobile shales as seen on flanking the seaward side of minibasin 4. Seismic units 2 – 6 are composed of interbedded layers of shale and sandstone. The strata filling the basin are uniform with strata onlapping and pinching out at the structural highs created by the salt. No MTC depositional systems are seen in minibasin 4.

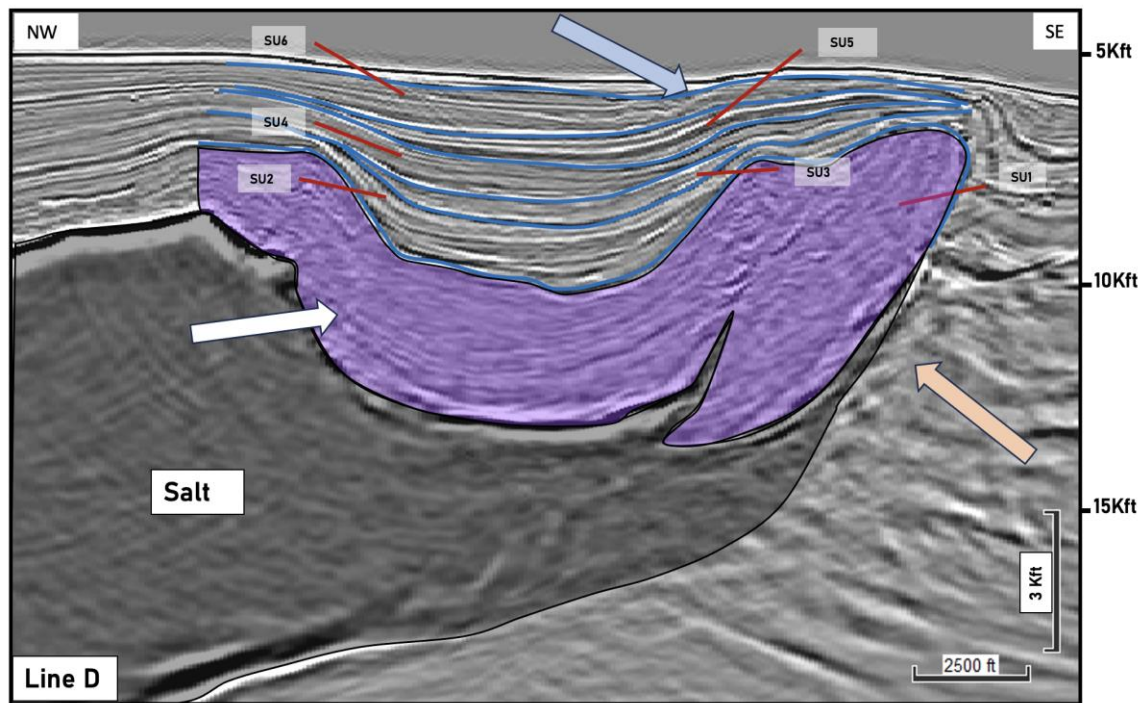


Figure 19. Seismic section of minibasin 4. Location of this line (Line D) is shown in Figure 15. Large mobile shale unit in shaded purple (white arrow), roof edge thrust created by the shortening event on the canopy edge (orange arrow), seismic units onlapping and thinning towards the salt high (blue arrow).

7.2.5 Minibasin 5

Minibasin 5 is a secondary minibasin, approximately 6.1 km across in diameter (Figure 20). The presence of symmetrical, bowl-shaped packages indicates minibasin 5 initially subsided vertically and was flanked by passively rising diapirs during the early-middle Pleistocene. The presence of tapered CHSs indicates sediment accumulation rate exceeded the diapir rise rate at this time (Giles and Rowan, 2012). This high sediment accumulation rate may reflect a high sediment supply rate, which may itself reflect the proximity of the study area to the Mississippi River, which at this time delivered large volumes of sediment to upper slope minibasins (Galloway, 2001; Galloway et al., 2000).

The basin is composed of 12SU, all thin towards the salt high. SU1 is split at the deepest point and is being introduced the salt canopy. The split in the unit is from the mobilization of the salt canopy and the overlying strata. SU2 penetrates SU1 at the point of separation resulting in the inclusion seen within the salt canopy. The salt canopy has few internal reflectors while the inclusion has a distinct top and bottom surface that is seen in the salt. Four MTC systems are found, the units display seismic transparency with chaotic reflectors. The units are separated by layered reflectors showing times of increased and decreased sedimentation. Within the minibasin a channel is seen eroding SU6, there is a distinct depression in the upper surface with the characteristics of a fluvial channel.

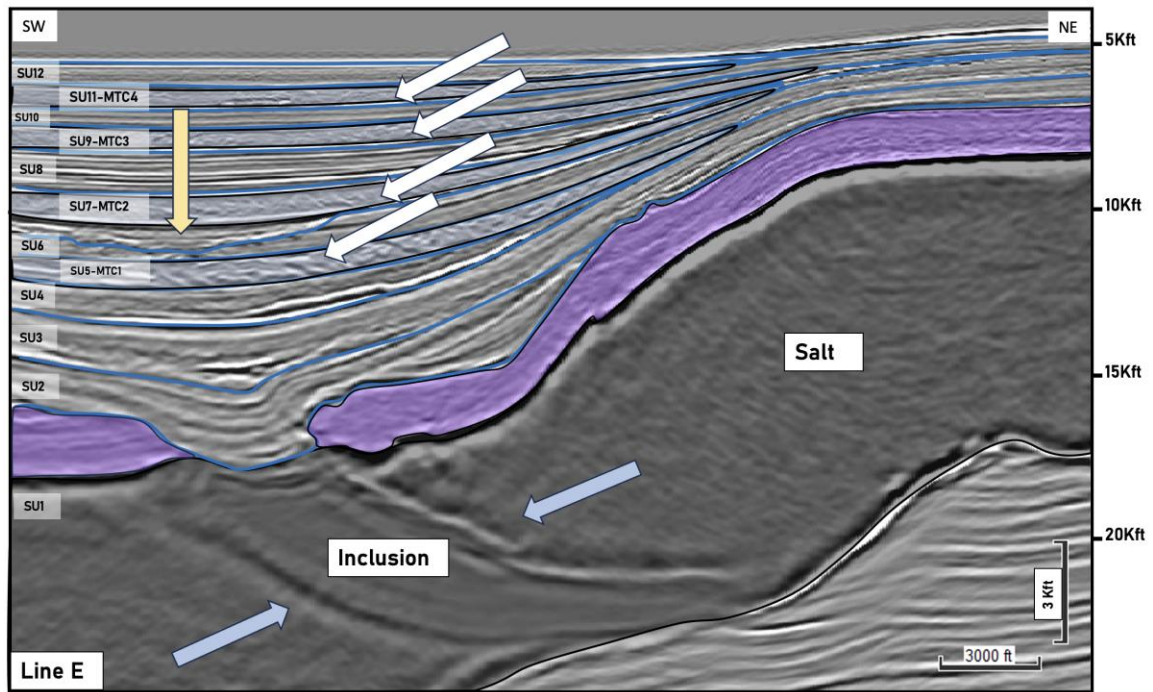


Figure 20. Seismic section of minibasin 5. Location of this line (Line E) is shown in Figure 15. Four MTC systems are seen to thin towards the NE (white arrows). The eroded top surface of SU6 outlines the base of the channel (yellow arrow). Top and bottom reflectors of the inclusion found within the salt canopy (blue arrows).

7.2.6 Minibasin 6

Under the salt canopy exists a primary minibasin that covers approximately 180 km² of our dataset (Figure 21). Seismic horizons T1-T4 are found within the basin (Figure 22). The basin commences directly above the Louann Salt, beginning with the Cretaceous unit overlaid by the Paleocene – Eocene, followed by Oligocene strata and then the lower Miocene that terminates against the lower base of the canopy. The strata overlying the basin have caused the salt to be displaced creating an elongated bowl-shaped basin where the majority of the minibasin is surrounded by the Louann Salt. The

megaflap located on the east side of minibasin 6 results form a tectonically active setting as the minibasin was forming. The northern and western flanks of the basin are entrained by the advancing salt body creating compressional forces from the west to the east. To the south, seismic units T1-T4 thin and pinch out towards a structural high from a salt ridge. The basin contains continuous stratigraphic sequences that are characteristic of the primary minibasins situated in the salt stock canopy province of the eastern Green Canyon (Pilcher et al., 2011). These sequences created desired reservoirs that are capped by the base of the salt canopy.

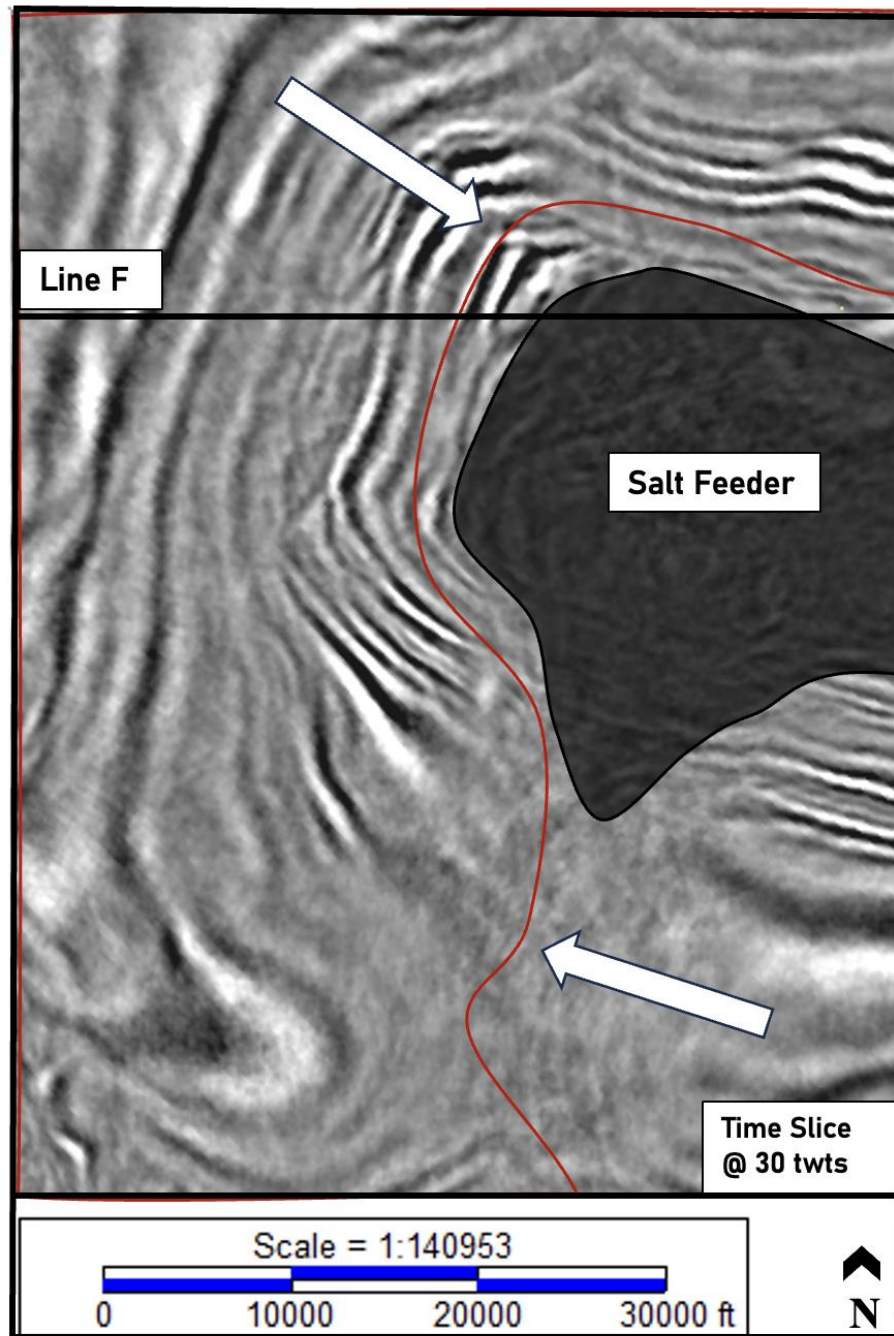


Figure 21. Time slice @ 30 [Kft]. Shaded dark grey area is the salt feeder limits, and red line (white arrows) outlines the extent of the primary minibasin.

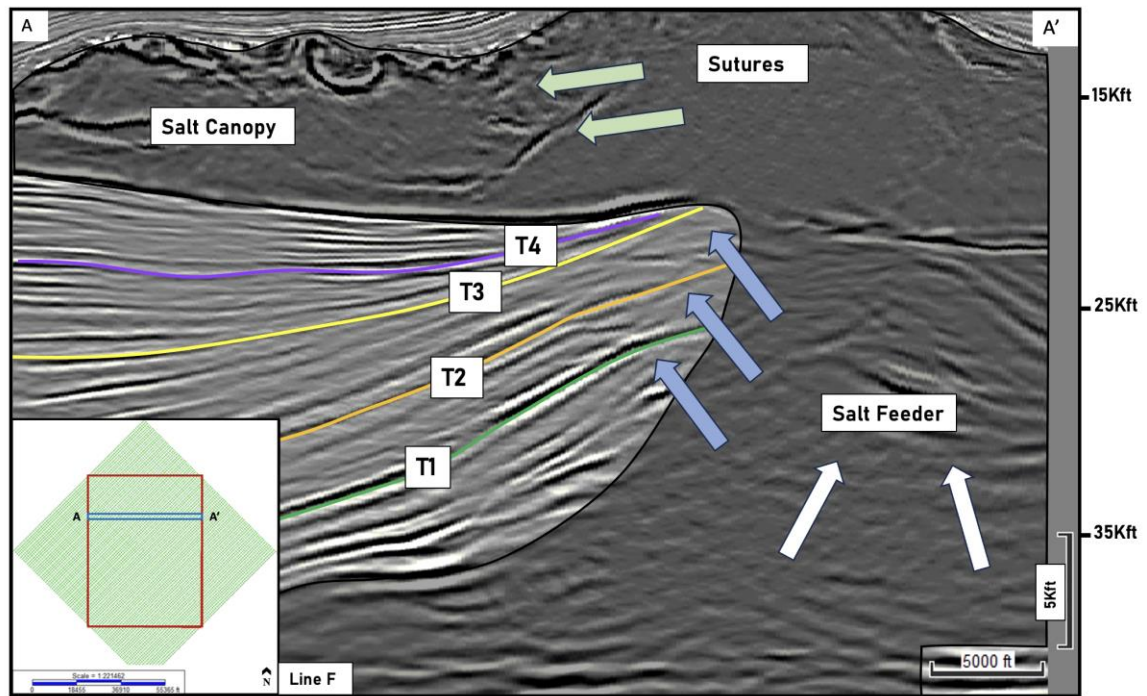


Figure 22. Minibasin 6. Location of the line (Line F) in Figure 21. Seismic Horizons, T1– Top Cretaceous. T2 – Top Paleocene – Eocene. T3 – Oligocene. T4 – Top lower Miocene. T1 – T4 seismic units thin and onlap the flanks of the salt feeder (blue arrows). Sutures located in the salt canopy (green arrows). White arrows denote direction of salt movement.

7.3 Megaflaps Puma Diapir

In the Puma Diapir, there are two megaflaps located on the southwestern edge of the salt feeder T1 and T2 (Figure 23 and 24) have been rotated to near 90° marking the sediment layers that define the top and base of the megaflap encasing the primary minibasin. The rotation of the layers creates potential reservoir and seals as the strata creates an impermeable layer against the rising salt (Jackson and Hudec, 2017).

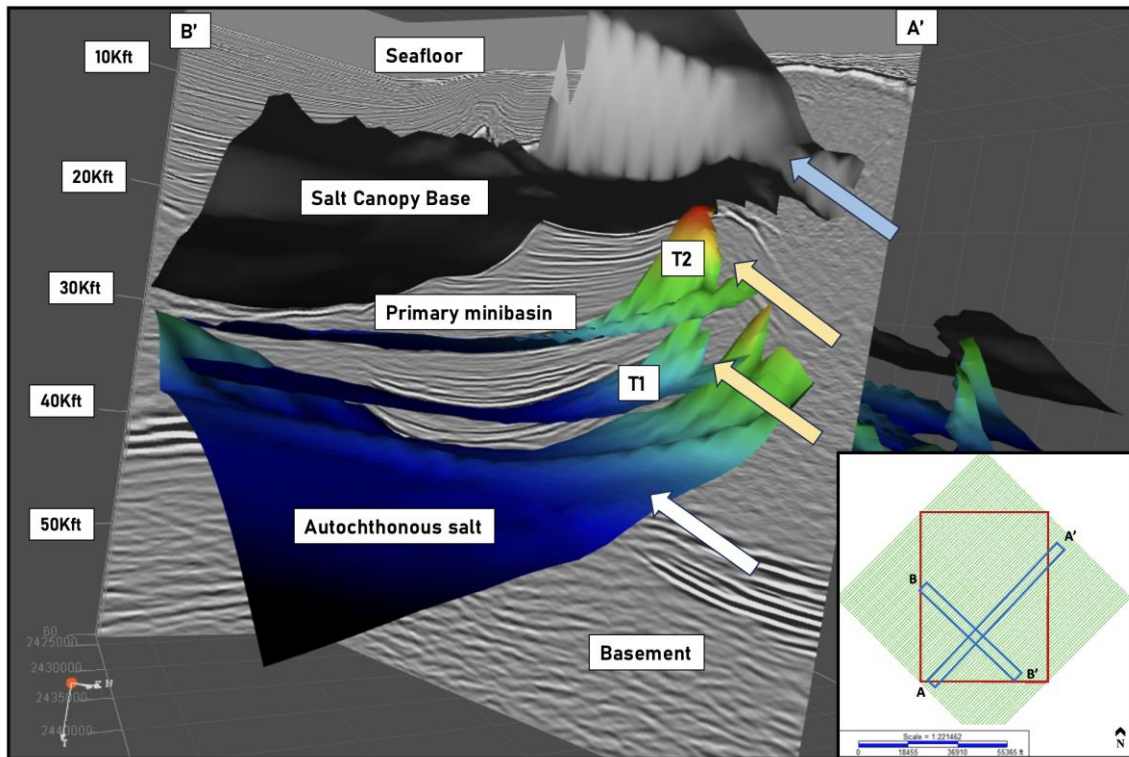


Figure 23. Section from Kingdom suite software in 3D post migrated data. White arrows pointing to the base autochthonous salt. Yellow arrows pointing to T1 and T2 seismic units. The units are overthrusting creating a megaflap. Blue arrow pointing to base of the salt canopy. Section from Kingdom suite software in 3D post migrated data.

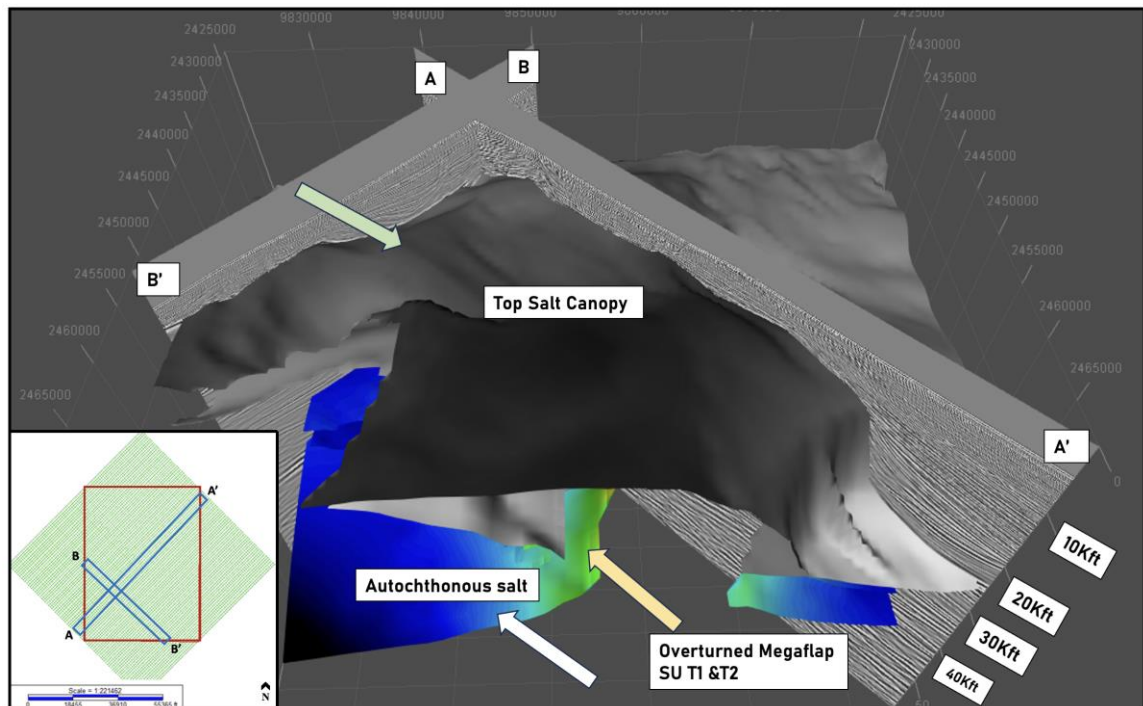


Figure 24. Top of salt canopy limits in the AOI. Seismic units 1 and 2 are located under the salt canopy (yellow arrow). The base salt is the lower most and is the bottom surface for the megaflap (white arrow).

7.4 Salt Feeder Puma Diapir

Attempting to interpret salt feeders can be challenging due to the limitations of the interpretation software and the complex geometries produced. To overcome the challenges discussed above, multiple horizons were used to map the lower and upper flanks of the feeder in the Puma Diapir (Figure 25). To locate the salt feeder, the base of the salt canopy was picked on the soft reflector across the survey. A gap resulted in the base of the salt that is determined to be the top of the salt feeder (Figure 26). Interpretation of the base and flank limits was based on zones of poor seismic reflectivity

terminating against horizontal reflection. This proved to be challenging on the southwestern side of the feeder where a megaflap was determined to be located. The feeder's base is found on the northern end of the data set, about 40 Kft, flanks of the salt are near vertical that terminate at the salt canopy base.

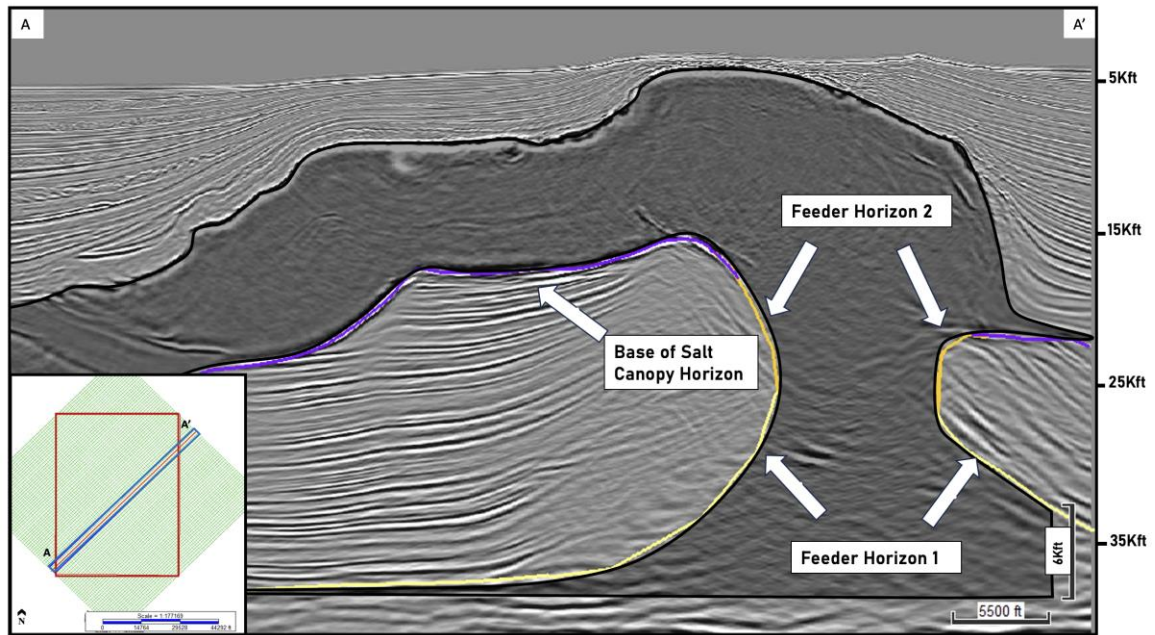


Figure 25. Salt Feeder limits, Horizon 1 light yellow, Horizon 2 in golden yellow. Feeder Horizon 1 was used to map the lower flanks until the limits of the horizon tool were met, at which Feeder horizon 2 was used to map the upper limits of the near vertical salt.

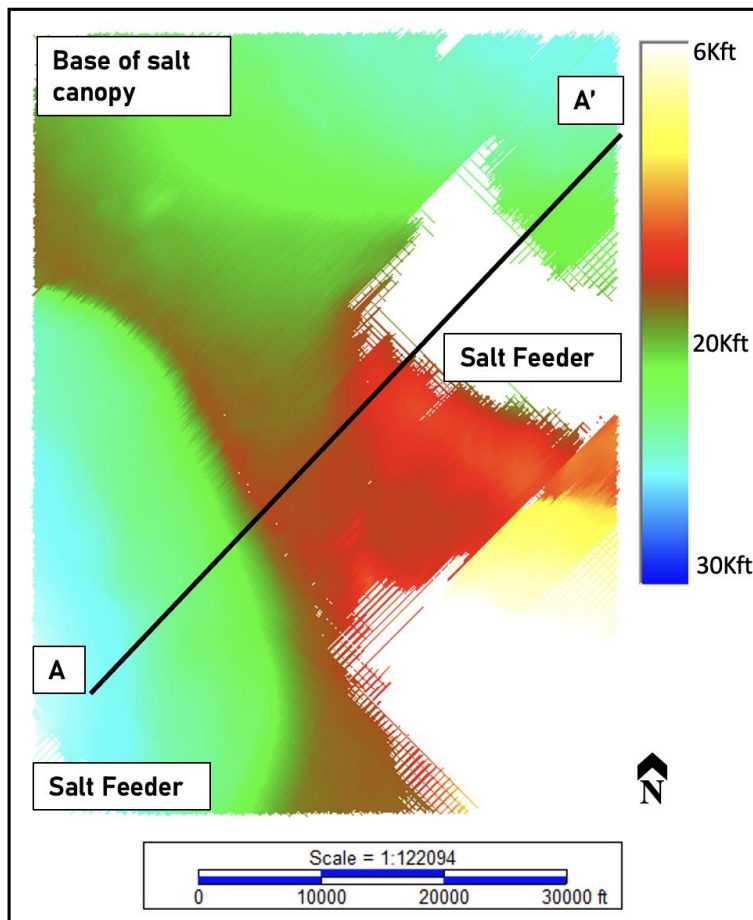


Figure 26. Map showing depth in time to the base of salt canopy, that was mapped on the soft reflector across the dataset interpreted to be the base of the salt. The area labeled salt feeder outlines the point at which the salt is dipping downward, and no longer parallels the sea floor.

7.5 Salt Welds Puma Diapir

Within the survey there are two salt welds. The First was in the southwestern section of the AOI at approximately 34 Kft and is found to be the base of the enclosed primary minibasin. The primary weld was formed from the loading of sediment causing the salt to be mobilized away from the depocenter of the minibasin (Figure 27). The

second is a tertiary weld found on the northeastern flank of the Puma Diapir (Figure 28). This weld is the base of minibasin 1 and formed from the continual loading of sediment resulting in a salt withdraw minibasin.

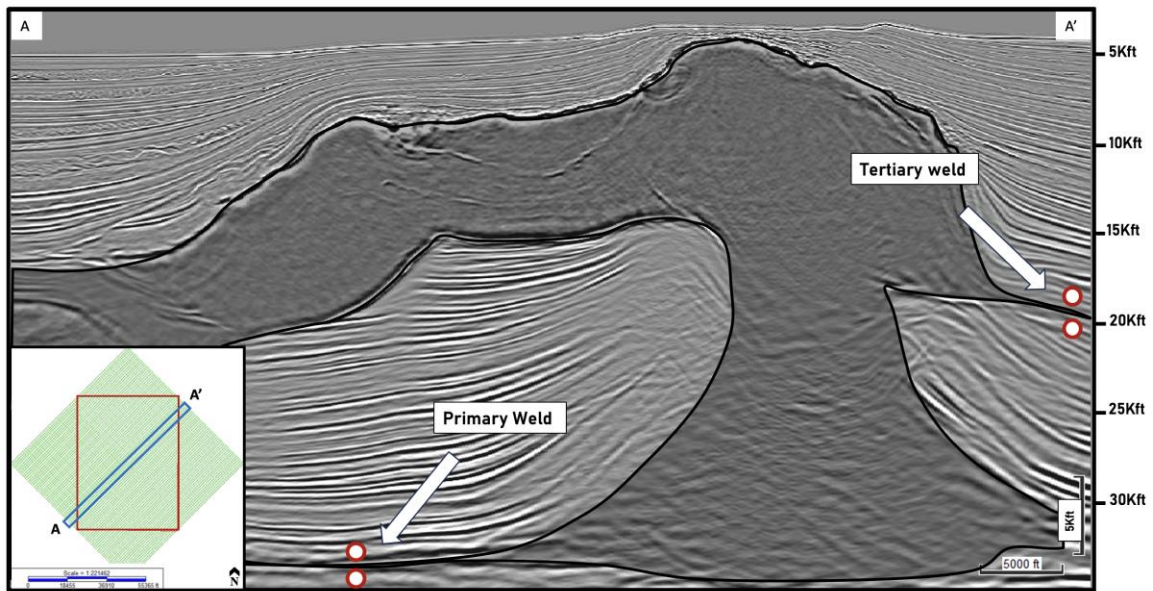


Figure 27. Salt in shaded grey area. Location of welds visible in our data set, noted by the two white dots.

7.6 Salt Body

There are two major salt bodies found within the AOI, labeled A and B throughout. Salt Body A is found on the eastern side of the AOI, and Salt Body B on the western side (Figure 28 and 29). Salt Body A is the smaller of the two seen in AOI, the salt originated from the autochthonous salt that was first mobilized during the Oligocene (T3) as the large amount of sediment influx continued through the Miocene (T4-T5) causing the salt to move towards the seafloor. Salt Body B is located on the northern end

of the dataset and covers most of the AOI. Salt Body B has a well-defined salt feeder that was initiated during the Oligocene (T3), continual sediment through the Lower Miocene (T4) moved the salt towards the surface and was capped by the Middle and Upper Miocene sedimentation. During the Miocene – Pleistocene the two separate salt body came in contact, creating a basal suture point, a characteristic feature noting the coalescence of separate salt bodies (Martin and Hudec, 2017). The movement of the salt alongside sediment deposition created various autosutures and allosutures seen throughout the interpreted seismic sections (Figure 17, 18 and 36). Within the salt canopy an inclusion is seen in the southern end of the visible seismic where Salt A encounters Salt B. The inclusion does not express the same transparent reflection seen in the salt canopy, instead it has a distinct top and base with some internal reflection that parallels the top and base.

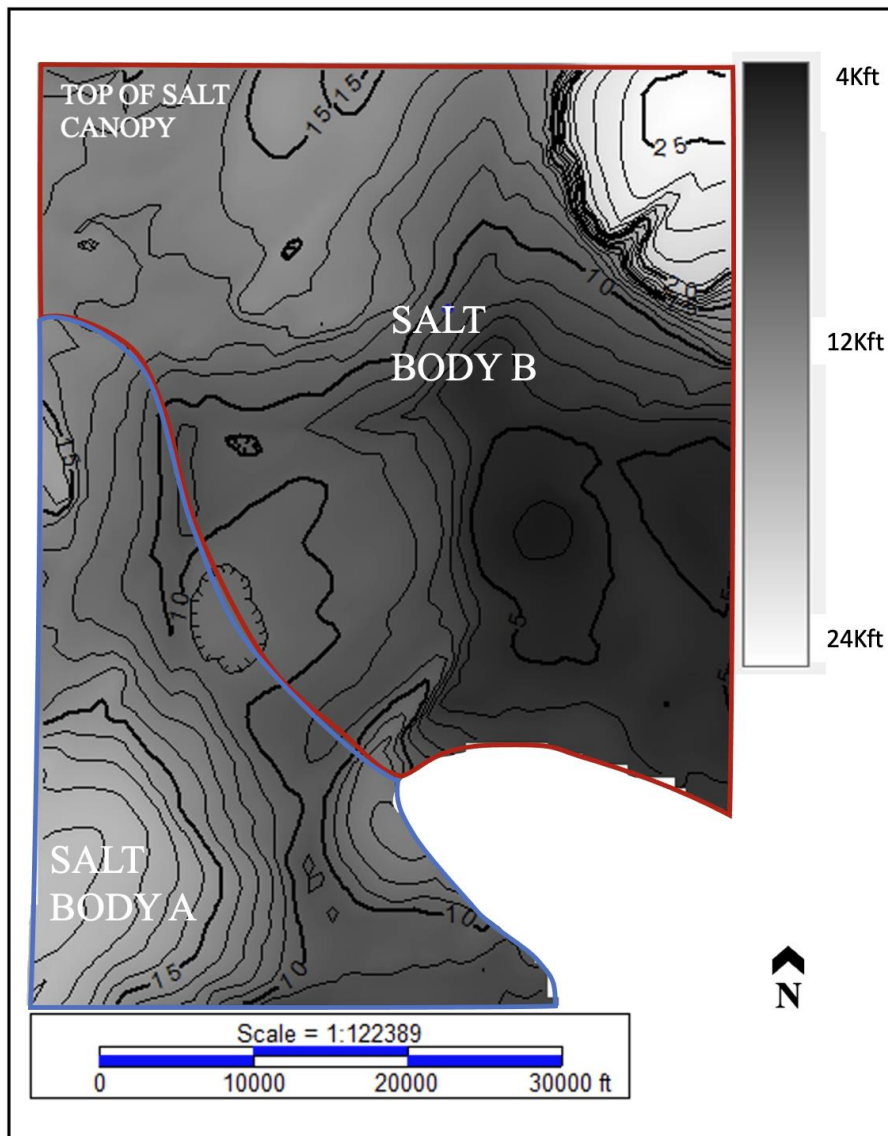


Figure 28. Map of top of the salt canopy in Kft. Approximate location of Salt Body A is outlined in blue and located in the southwestern portion of the study area. Salt Body B is outlined in red and located to the northeast.

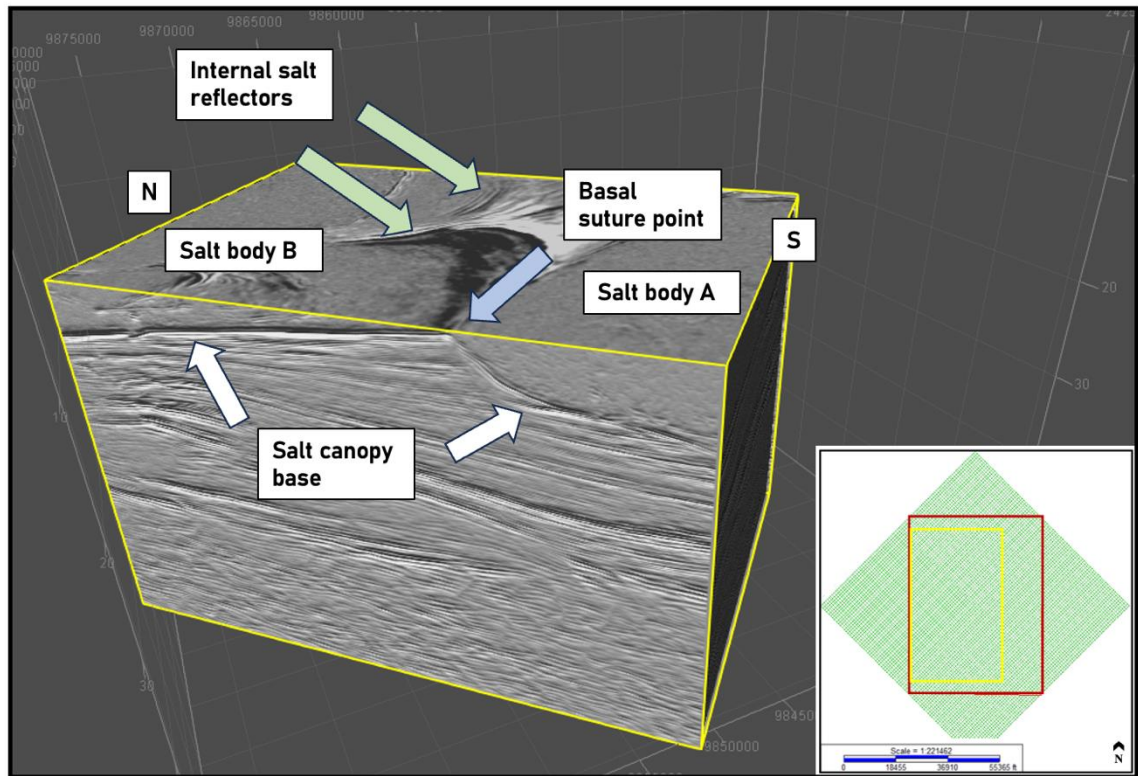


Figure 29. Cubic Volume of 3D seismic, the extent of viewed section is outlined in yellow within the AOI. Seismic has been reprocessed to enhance relief of the reflection surfaces. The base of the salt canopy (white arrows) is easily distinguished from the underlying reflectors with the enhanced reflection. Salt body A is encountering the Salt body B, creating a basal suture point (blue arrow). Internal salt reflectors at the top of the time slice are identified by the green arrows.

7.7 Faults

Sediment loading along with other large scale regional stresses and motion have disrupted the underlying strata. The lateral and upward motion of the autochthonous salt has created an array of large-scale regional faults that span hundreds of feet to smaller scale local fault systems (Figure 30) that share a common strike and dip. The seismic

dataset allows for the tracing and mapping of the subsurface faults (Figure 31). The increased resolution of the seismic has enabled small-scaled faults to be seen that were not able to be resolved in earlier data sets. The fault map allows for and an increased understanding of the structural concept between salt and clastic sediment interplay, therefore enabling advancements in understanding subsurface tectonic systems and their effects on hydrocarbon exploration. Faults were abundant and well imaged as many of them were shallow and located above the salt canopy. A total of 27 faults to the north. 10 are located on the southern end of our data set. Thirty-seven normal faults were mapped in the kingdom suite software. The software can trace along the faults, compile the data and represent the finding in histograms and rose diagrams (Figure 32).

The faults were all located above the salt canopy. Faults on the southern limits of the salt (Salt A) were active during the Pliocene – Recent as indicated by the faults cutting through the Pliocene, Pleistocene and Holocene aged sediments. These faults are smaller in comparison to the faulting founding towards the north above salt body B. Faulting in the northern area are rooted at the top of the salt canopy and terminate in the recent age sediment with the exception of a few faults located within minibasin 3 zone. The faults cross Upper Miocene, Pliocene, Pleistocene and Holocene aged strata (Figure. 31). Faulting occurring from Upper Miocene to Pleistocene, seismic units maintain same thickness across fault plane meaning movement occurred after deposition of these sediments and ceased during recent- Holocene.

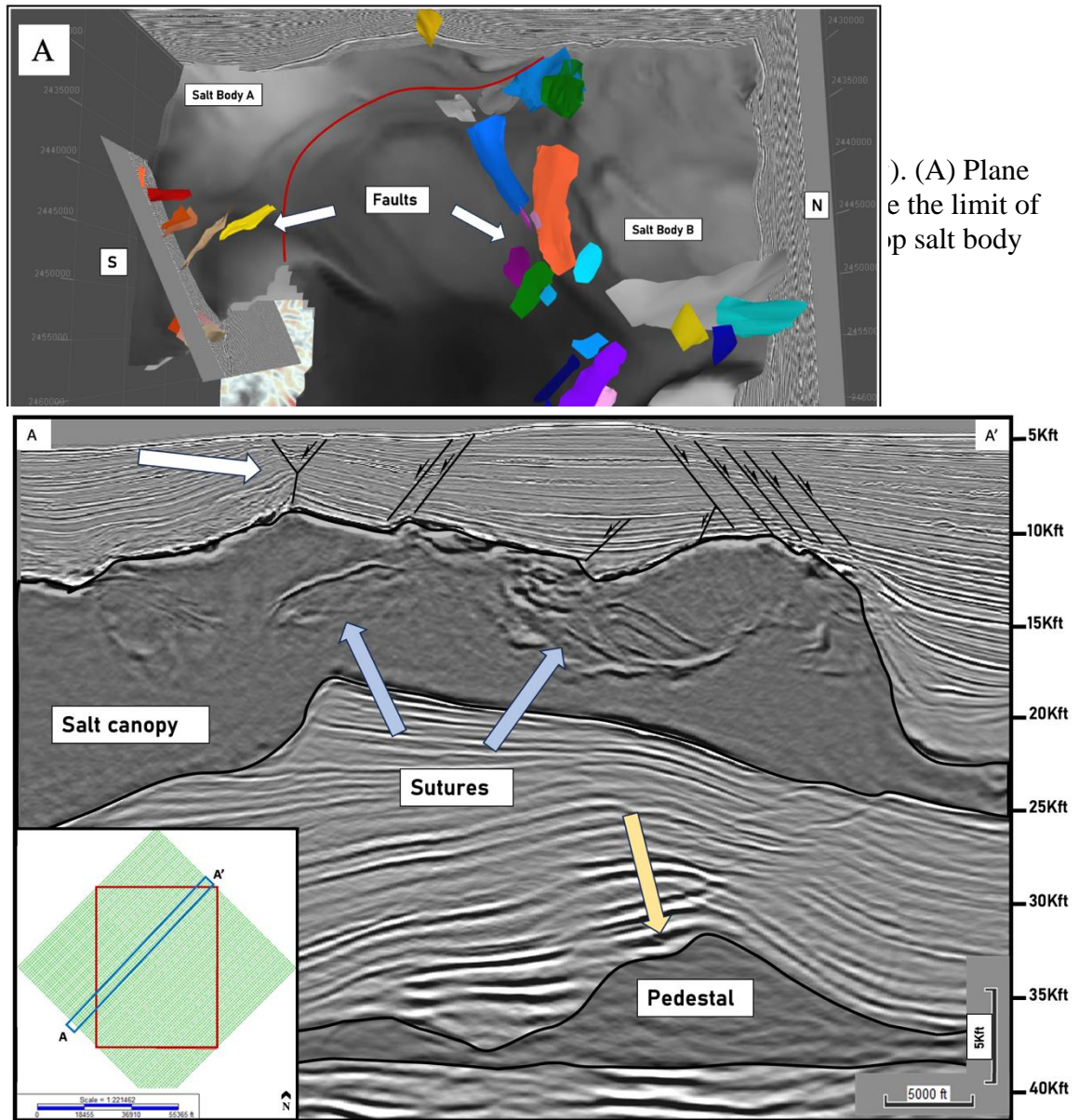


Figure 31. Regional 3D time migrated data, salt limits outlined in shaded grey. Strike-slip system is located towards the seafloor on the southwestern end of the seismic profile (white arrow). Reflectors within the salt canopy denote sutures (blue arrows). Salt diapir pedestal located under the allochthonous salt (yellow arrow).

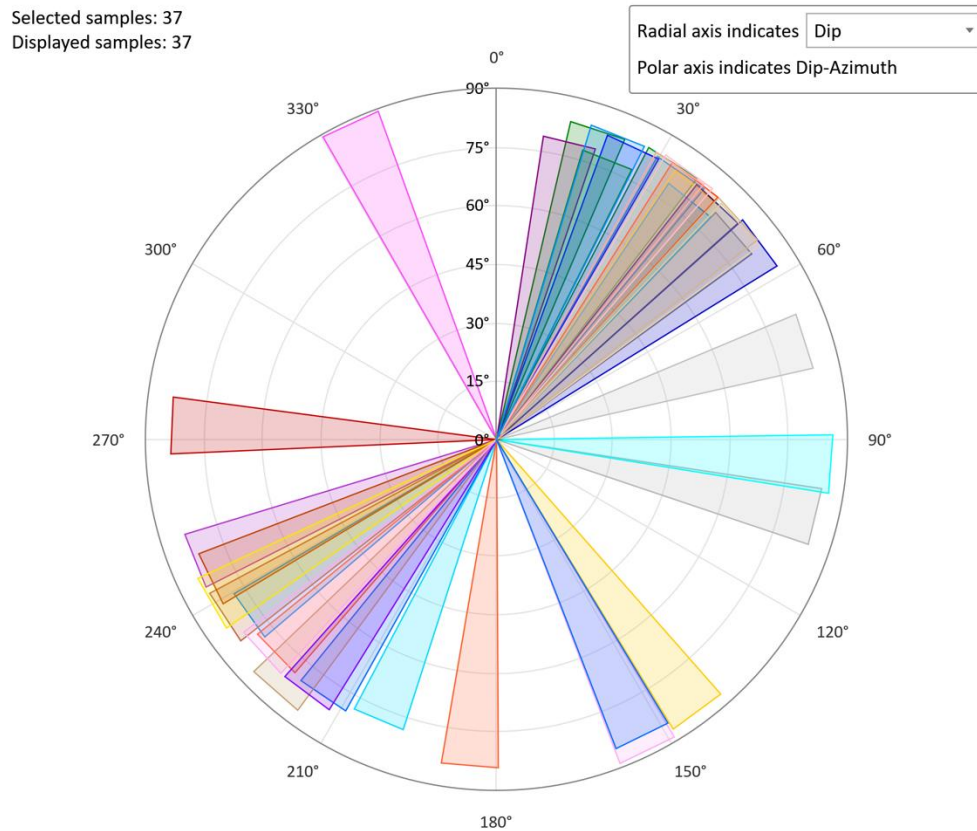


Figure 32. Rose diagram from generated by Kingdom Suite using the faults mapped in the dataset. Diagram shows dominate strike trend for the faults, and dip.

7.8 Frontal Thrust Systems

The salt sheets that are located on passive margins above a bathymetric high and are generally found above a salt feeder that causes the salt to mobilize. Gravity spreading is common around the canopy rim producing thrust faults. Canopy margin thrust systems are composed of three parts. Most will contain a roof-edge thrust that will separate the

condensed strata located above the salt from the thicker strata located in front of the thrust.

The edge of the salt canopy on the southeastern edge of the Puma Diapir is an example where the edge of the salt canopy has begun to move upwards towards the sea floor (Figure 33). The second common feature is the roof edge thrusts result in an imbricate wedge system. The sediments in front of the roof thrust are compressed resulting in an accumulation of sediment in front of the thrust (Figure 34). Lastly, salt-roof thrusts shorten the strata located on the roof of the salt sheet. The shortening located in these systems has resulted in sediment accumulation anticlines and synclines above the salt.

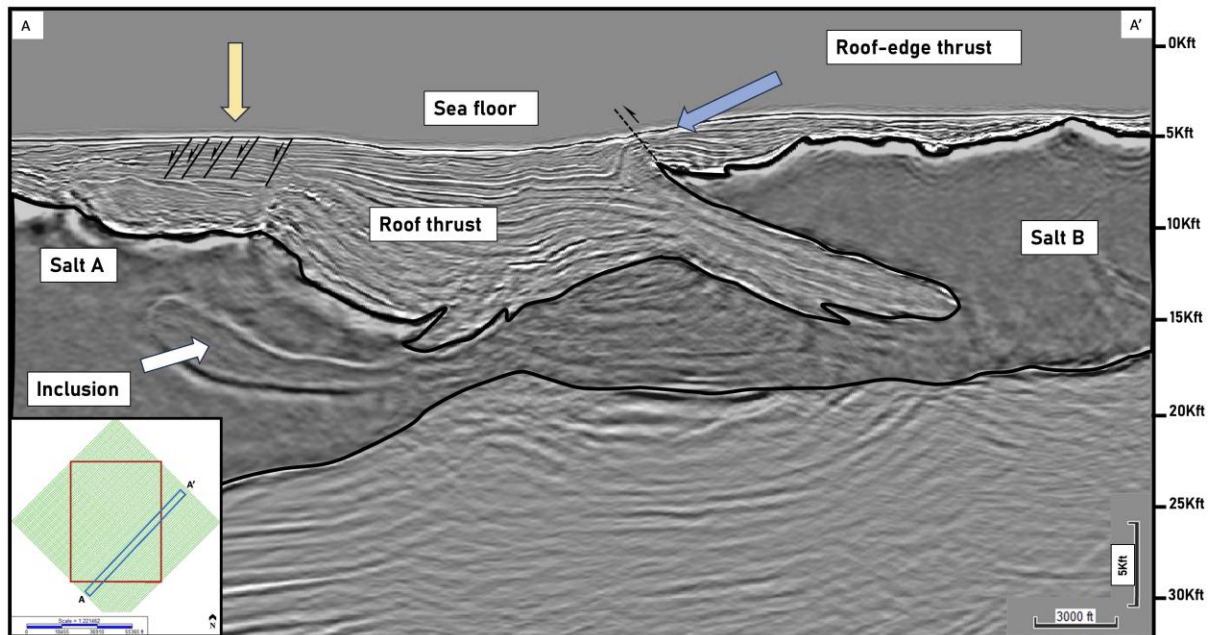


Figure 33. Salt body A to the left Salt body B to the right, Roof-edge thrust towards sea floor (blue arrow). Echelon extensional faulting is found above salt body A (yellow arrow). The inclusion found in salt body A is easily distinguished from the seismically transparent salt (white arrow).

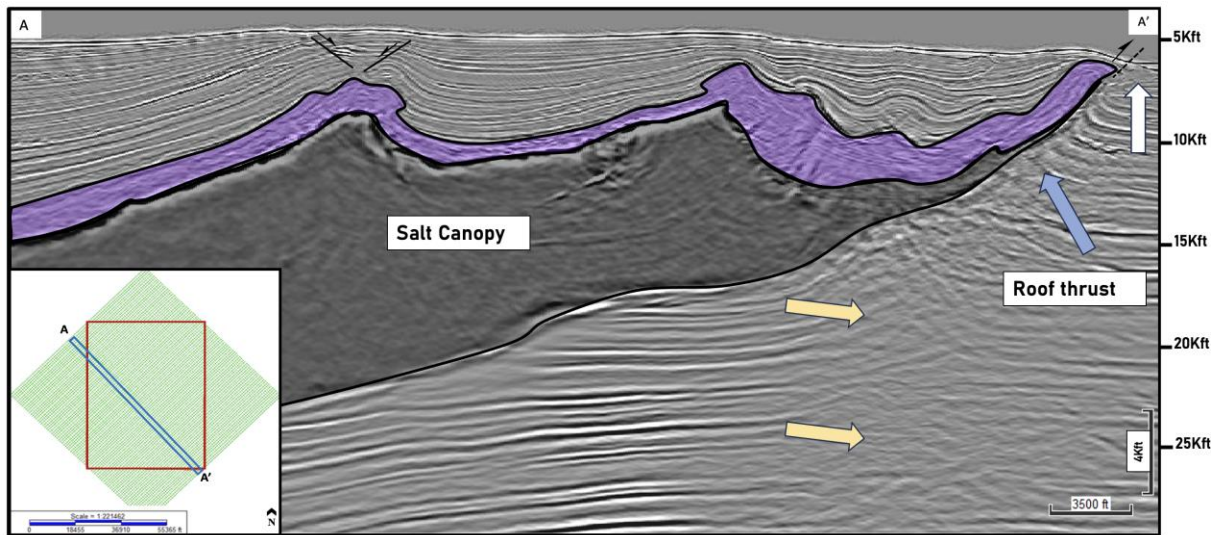


Figure 34. Shaded Purple defines transparent mobile shale. Shades grey marks the extensional salt rollover note prominent roof thrust (blue arrow) system toward the southeast. There is a seismically transparent zone underneath the tip of the roof thrust (yellow arrow). Sediment accumulation occurs in front of the thrust (white arrow).

7.9 Mobile Shale

The mobile shale in our AOI is thickest and most abundant towards the west end of the data set (Figure 35). Where most abundant, thickness are found to be from three Kft and where salt rise has outpaced sedimentation, the shale thins against salt highs. Thinning of the shale trends southward as the shale thins and onlaps the salt canopy. Extensional faulting dips towards the northwest and cuts across the shale. The distribution of the shale suggest it was deposited as one continuous unit that has been reworked by the active and passive stages of diapirism and is now found in the lows created by the rising salts. The steep faulting above the salt is created by the rising salt

and further emphasizes the distribution of the shale in where the downthrown blocks and lows contain the shale.

Line 6501 (Figure 36) highlights the area where the shale is located above the canopy along where the shale is absent. Throughout the dataset it is noted that the areas where a relatively thick shale unit is found, the top of the salt canopy is well defined and sharp. Areas of thin shale are seen to overlay a chaotic salt canopy top. The top of the salt is not well defined and instead is found to be jagged and erratic. Within the salt, the areas with thin to missing mobile shale have an increase in reflectors that are concentrated towards the north side of the dataset.

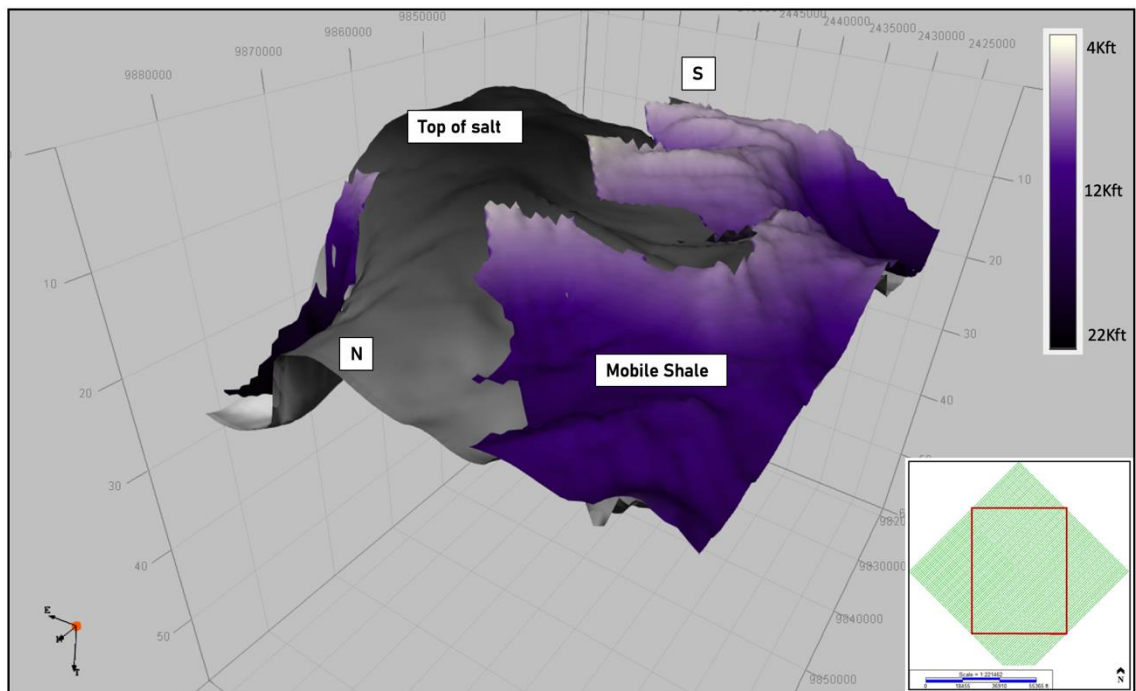


Figure 35. Limit of mobile shale found above the salt canopy. The shale is found mostly in the lows from rising salt.

Discussion is still on going on what is the cause for mobilization and how the shale behaves within different structural regimes (Hudec et al., 2023). Here we note the chaotic top surface of the salt canopy that is inferred to be a result of the mobilized shale. Pressure of the overlying sediment is thought to be the main mechanism for salt mobility being incorporated within the salt body and the driving force for the movement of shale.

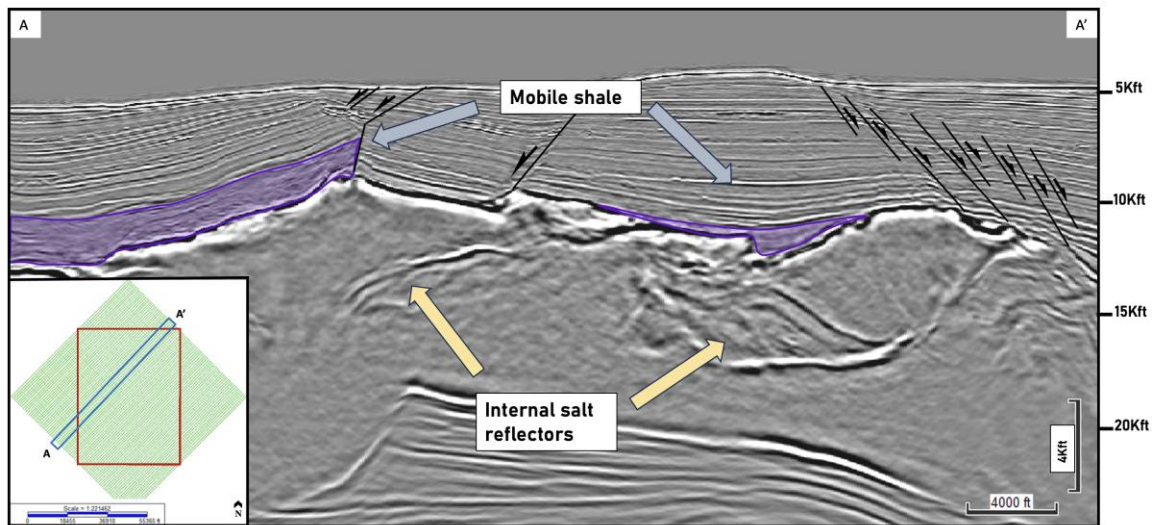


Figure 36. Line 6501. Areas with lower amounts of mobile shale shaded in purple (blue arrows) correlate with increased amounts of intra salt reflections (yellow arrows) identified as sutures.

8. DISCUSSION

The Puma Diapir, located near the Sigsbee Escarpment, contains complex structural and sedimentary features due to the continued movement of the Louann Salt in the region. In the AOI, six different time periods marked by the enhanced reflection of the strata in the seismic dataset were identified (Figure 14), two salt feeders, six minibasins, numerous extensional and thrust faults, two welds, and an extensive mobile shale unit overlying the salt bodies. The Puma Diapir has undergone multiple stages of active and passive diapirism, as described by Rowan and Giles (2011).

8.1 Puma Diapir Evolution

As the North American plate separated from the Yucatan and South American plates, a shallow basin was created with a connection to the Pacific Ocean across the central part of Mexico. The result was deposition of as much as 4 km of nearly pure halite precipitated creating the Louann Salt (Galloway, 2008). The large size, location, and physical properties of the mother Louann Salt have altered the depositional patterns as the malleable evaporite body shifted and moved throughout geologic time. The movement of the salt is not assigned a specific time period, as sediment loading is the main driving mechanism of the salt body and is an ongoing process near the edge of the Sigsbee Escarpment. Here a reconstruction of the Puma Diapir highlights the various stages of active and passive diapirism that coincide with the associated geologic times.

T1 -Top Cretaceous

T1 is marked by passive diapirism (Figure 37). Deposition over the mother Louann Salt initiated in the Cretaceous. Lower Cretaceous strata consist of the Norphlet, Smackover, and Cotton Valley formations that form the tectonostratigraphic mega sequence overlying the initial topography by the initial break breakup unconformity, the upper records the termination of seafloor spreading. Several small alluvial fans, braid plain, and delta systems along with eolian, sabkha, and playa deposits are found noting the aridity of the shallow gulf basin. The Oxfordian Smackover, Buckner, and Gilmer formations started the first carbonate-dominated deposition of the GOMB.

Subsequent sediment deposition during the Late Jurassic and into the Cretaceous resulted in salt mobilization due to sediment loading. The sedimentation during the cretaceous covered the majority of the Louann with deposition of sediment as much as 300m (Sohl et al., 1991; Galloway, 2008) The Cretaceous aged units are seen overlying the autochthonous salt throughout the dataset where the salt has vanished as seen in the strata directly above the primary weld in minibasin 6.

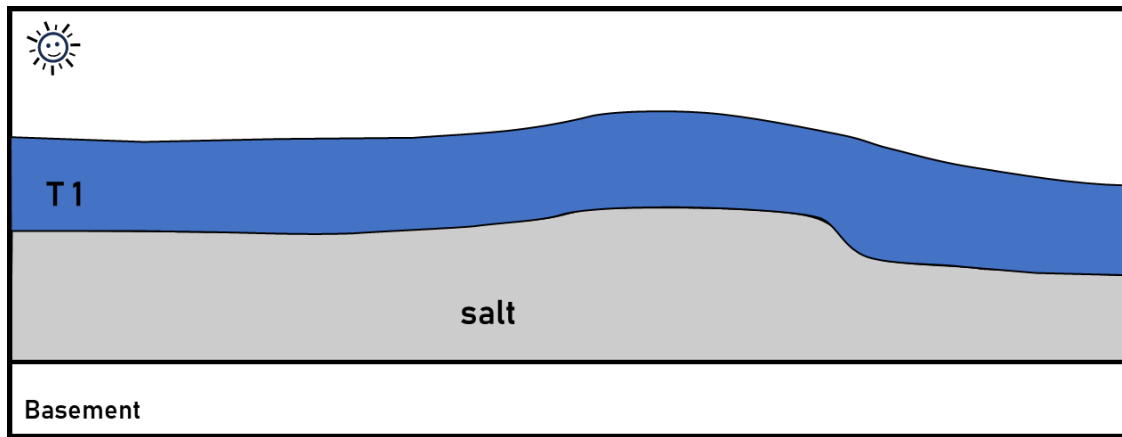


Figure 37. Diagram of the Puma Diapir during the Cretaceous, showing passive diapirism. The massive Louann Salt was deposited over preexisting basement rock during the Middle Jurassic (Bajocian; ~162-163 Ma (Hudec et al., 2013)).

T2 - Paleocene – Eocene

T2 is marked by active diapirism (Figure 38) where the Paleocene- Early Eocene deposition records the increase in clastic supply from the advancing Laramide uplift originating in the Central and Southern Rocky Mountains that extended eastward into the Gulf of Mexico Basin, reflected by the broad folding of the Rio Grande Embayment (Galloway, 2005; Winker, 1982). The deep-water sedimentation dominated this time period fed by the surge of clastic supply from developing Laramide hinterland (Galloway, 2019). This period was dominated by deep water deposition of turbidites, gravity flows and submarine fan systems resulting in deposition of the Wilcox Group. Laramide compression – related episodes continued throughout the Middle Eocene creating zones of subsidence that was infilled by the continued Eocene deposition. The rapid sediment loading mobilized deep – water muds initiating the first of successive

Cenozoic phases of salt mobilization beneath the basin margin towards the paleo-continental slope (Galloway, 2008).

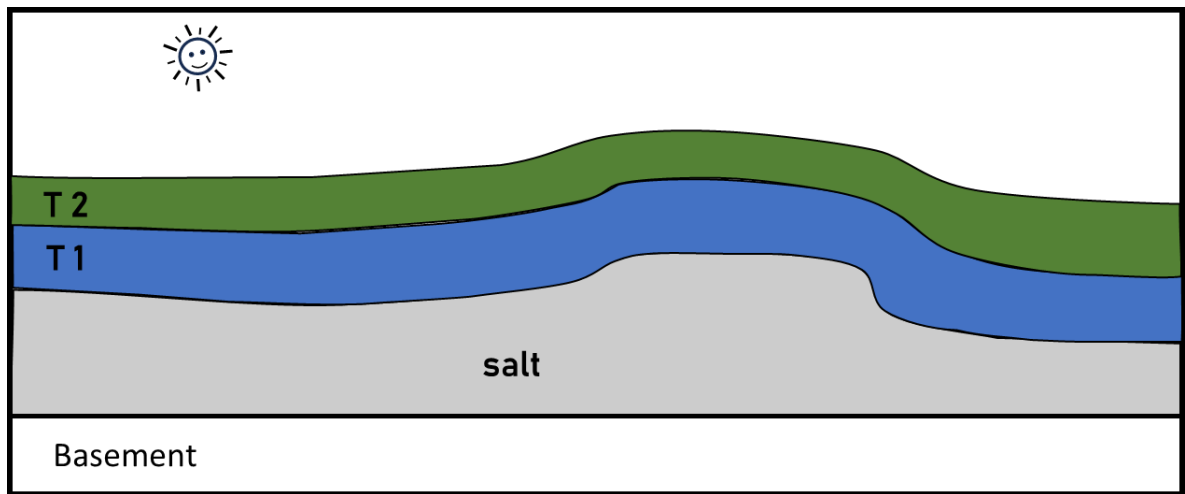


Figure 38. Diagram showing active diapirism during the Paleocene-Eocene. T1 – Cretaceous; T2 – Paleocene – Eocene. The increased sediment loading is the driving mechanism for salt motion during this time. Top of Paleocene – Eocene unit conformably overlying the Cretaceous units.

T3 – Oligocene

T3 is a time of diapirism (Figure 39) created by the massive amount of sediment influx into the GOM during the Oligocene (Galloway and Williams, 1991; Galloway, 2008). Crustal heating, uplift, and volcanism in northern Mexico and southwestern United States along with explosive volcanism and caldera collapse to the west led the way to the long-lived recycling of sedimentary rocks, volcaniclastics, and reworked devitrified ash that was deposited in the mid-Oligocene into the early Miocene ultimately

resulting in the Frio depositional episodes (Galloway et al., 2011). The Frio depositional episode was dominated by the progressive growth of four delta systems. The four delta systems continued to bring sediment to the basin for more than 10 million years depositing an average of 50,000 km³ of sand (Galloway et al., 2011). The regional thermal uplift alongside the large inputs of sediment created a time of reactive diapirism evident by minibasin 6 (Figure 21), where the filling of sediment thinned towards the top of the rising salt. The seismic units deepen towards the minibasin depocenter and thins against the salt feeder. The Louann has reached the surface and is flowing in specific areas at which the Frio deltas prograde into and cross the Houston salt basin, loading on sub-adjacent Louann Salt and creating a phase of reactive salt diapir growth and minibasin development (Diegel et al., 1995; Galloway, 2008).

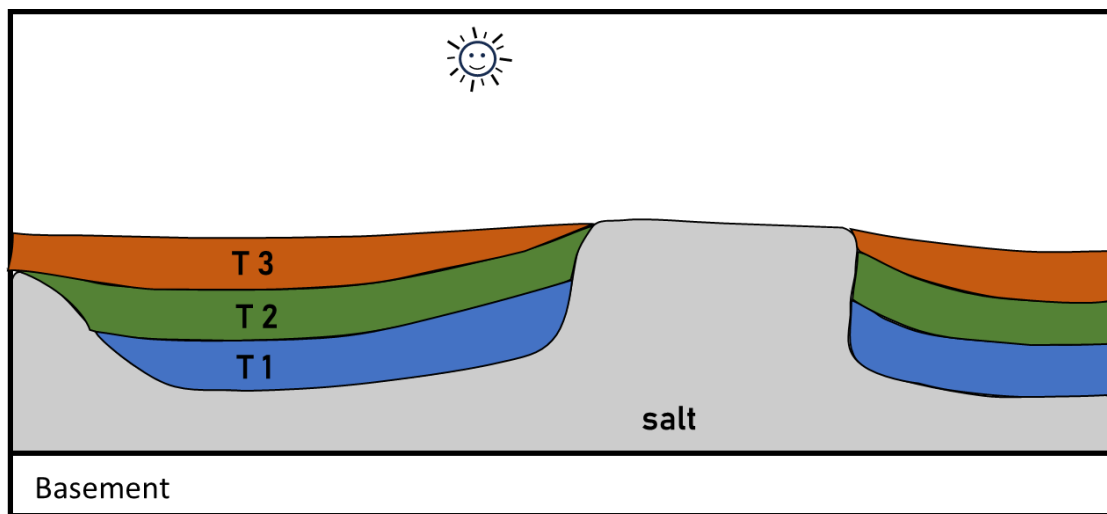


Figure 39. Diagram showing reactive diapirism during the Oligocene. T1 – Cretaceous; T2 – Paleocene – Eocene. T3 – Oligocene.

T4- T5 – Miocene

Miocene basin fill is a long-lasting multi-million-year depositional episode that records the deposition of the Gulf of Mexico from the Northwestern to the Eastern margins. The Miocene is broken up into two long lived episodes divided by a shorter episode. T4 is the upper limit of the short-lived middle Miocene and the long-lived Lower Miocene (Figure 40), and T5 is the top of the upper Miocene (Figure 41). The changes in the fluvial axis of the modern Trinity/Sabine River alongside the increased sediment input from the paleo Mississippi prograde the continental margin 65-80 km basinward along the Texas/Louisiana border (Galloway, 2008). The onset of the Red and Mississippi deltas resulted in hyper-subsidence and continental margin collapse creating large-scale salt withdrawals. This moved depositional loading eastward ultimately resulting in the collapse of the Planulina embayment, nearly seven km of lower Miocene sediment filled the central Gulf depocenter.

Sediment deposition accumulated along the continental margin and slope. The deposition created numerous amounts of minibasins and salt-cored highs that are filled by advancing delta-fed aprons (Prather et al., 1998; Galloway, 2008). In the relatively steep Northeast margin, turbidite channel complexes dominated the area and extended to the slope toe, initiating new submarine fan systems (Galloway, 2008). These systems fed large amounts of clastic sediments creating thick sequences that are seen in the lower units comprising minibasins 1,2, and 5. The large influx of sediments quickly covered the rising salt and deepened the minibasins. The thinning of the units towards the rising salt

is characteristic of the high deposition rates seen in the Miocene-aged strata in minibasins 1, 2, and 5. Sedimentary loading result in evacuation of salt the eastern limit of the salt canopy, later forming the tertiary weld surface that outlines the lower limit of minibasin 1. The weld was created by the Miocene deposition in the minibasin causing the salt to be mostly removed. At the end of the upper Miocene, T1-T4 has become an encased minibasin as salt moves laterally and upwards. Salt body A meets salt body B, and the creation of basal suture commences. The basal suture is situated in between the lower – middle Miocene and upper Miocene sediments.

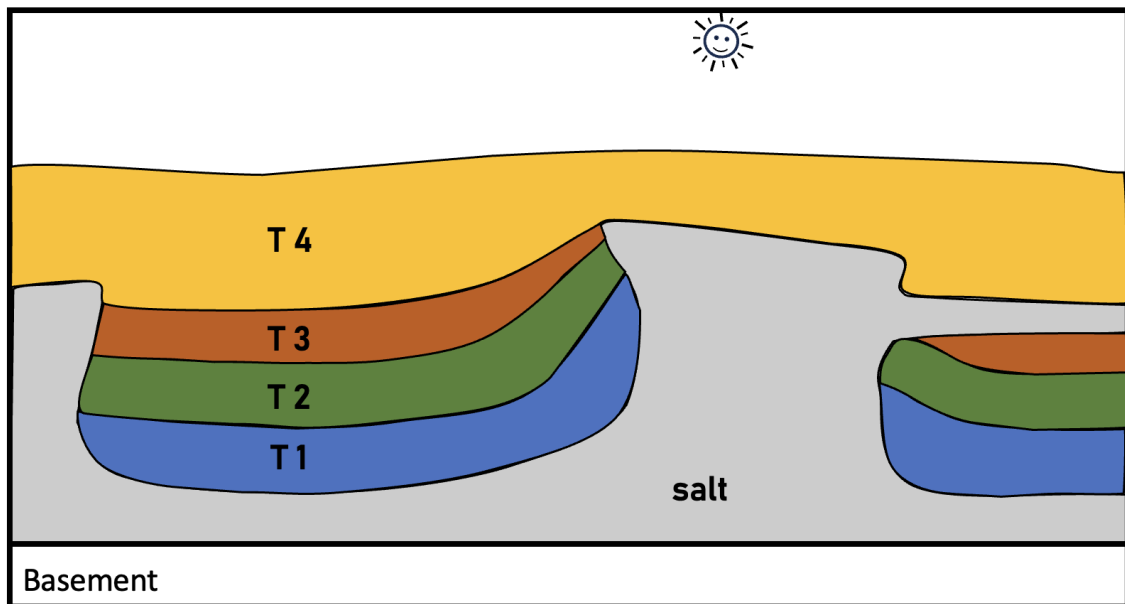


Figure 40. Passive – active diapirism (lower – middle Miocene depositional episodes) Diagram illustrating passive diapirism in the Puma Diapir during the Miocene depositional episodes. T1 – Cretaceous; T2 – Paleocene – Eocene. T3 – Oligocene. T4 – Miocene.

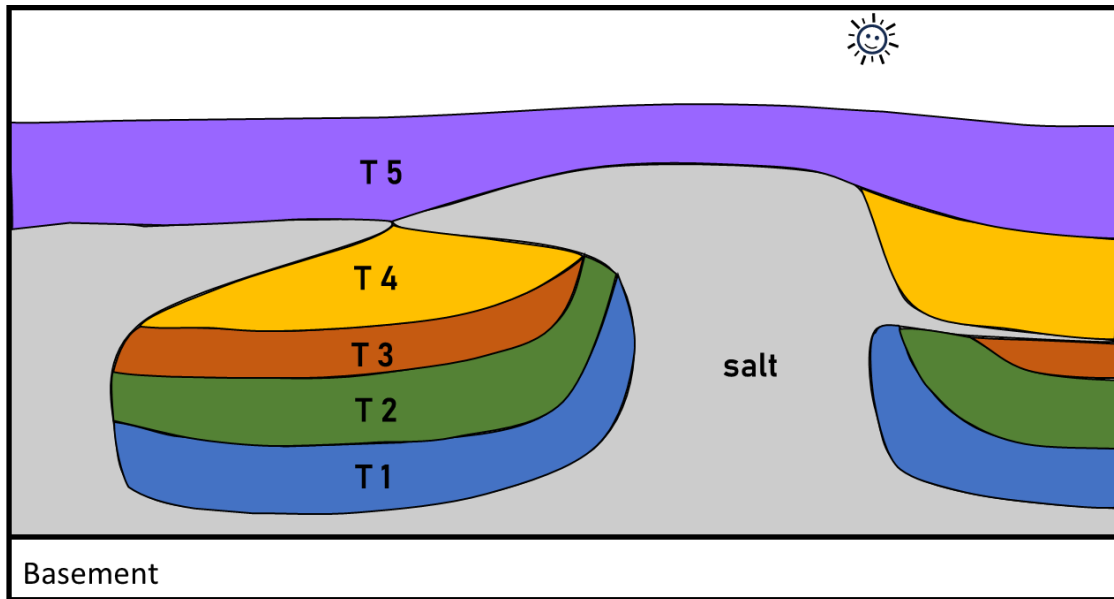


Figure 41. Diagram illustrating active diapirism during the upper Miocene. T1-T4 has become an encased minibasin, active diapirism forceful intrusion into overlying strata salt as sedimentation continues. Salt body A contacts salt body B, and the creation of basal suture commences. T1 – Cretaceous; T2 – Paleocene – Eocene. T3 – Oligocene. T4 – Miocene. T4 – Pleistocene.

T6 Pleistocene through Present Day

During the Pleistocene, instabilities associated with rapid shelf edge deposition, glacial outwash, and frequent sea-level changes resulted in a phase of mass wasting and submarine canyon erosion and filling. The east flank of the delta system located in the Gulf of Mexico is dominated by relatively short-lived canyons. The continual depositional loading of the shallow salt canopy has created the modern-day slope structures and the topography we see today (Figure 42). During these periods of active diapirism the forceful intrusion into overlying strata created numerous extensional faults

in the Pleistocene strata seen in all of the secondary minibasins (Figure 15, 16,17,18 and, 19). In Figure 36, faulting is rooted at the top of the salt canopy and ends at the base of the Holocene sediments.

Present day sedimentation continues to influence the Puma diapir, currently in a stage of active diapirism. The large amount of sediment loading, alongside a plentiful supply of salt has created a diapir that is nearly at the sea floor. The coalescence of salt bodies has created a salt canopy, where two main salt bodies were seen within the dataset; overlying sediment loading is has created five secondary minibasins that surround the diapir. The resulting coalescence of the salt bodies has created various sutures within the salt canopy along with important salt welds that two of the minibasin rest on. The sutures have been labeled where prominent as “Internal salt reflectors” Ex. Figure 29. The rise of the salt has caused the units directly about the autochthonous salt to be upturned created a megaflap adjacent to the salt feeder ultimately creating and enclosed minibasin. The coalescence of the salt bodies and the megaflap formation play a significant role in the reconstruction of the salt and surrounding strata shown in figures 37 - 42.

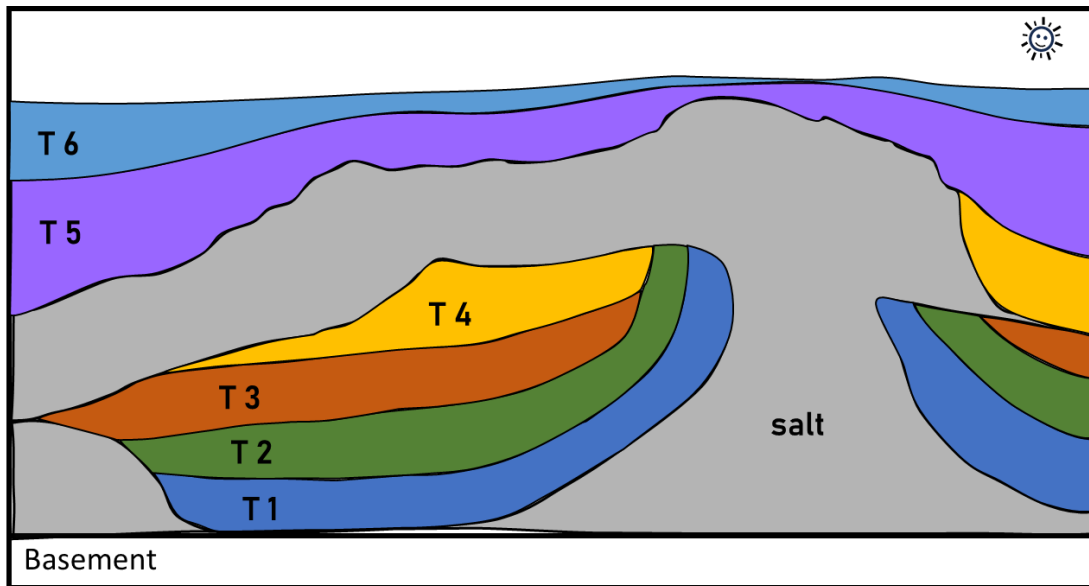


Figure 42. Diagram illustrating the modern structure of the Puma Diapir, undergoing active diapirism. T1 – Cretaceous; T2 – Paleocene – Eocene. T3 – Oligocene. T4 – Lower Miocene / Middle Miocene. T5 – Upper Miocene. T6 – Pleistocene – Recent.

9. CONCLUSIONS

The Puma Diapir is a mature structure that encompasses many aspects of salt tectonics, initiating from sediment loading of the Louann Salt causing the vertical and lateral movement of salt forming salt pillows and walls. The various stages of sedimentation have ultimately resulted in salt withdraw basin forming localized zone of salt welds in the salt located above the basement as well as the salt penetrating the Miocene sediments that surround the diapir. The various stages of active and passive diapirism are attributed to the availability of salt, the flow of salt and the large scaled tectonic activity of the GOMB. The study has highlighted these systems and have been interpreted on the dataset. Continual advancements in the geophysical world will allow for a better understanding in the development of salt influenced basin history, therefore improving offshore play development, and allowing for increased hydrocarbon production while reducing drilling hazards.

Reconstruction of major movements in salt and its resulting effect on the surrounding strata were shown with the corresponding periods of active and passive diapirism. The advances in seismic acquisition have made it possible to interpret the small defining characteristics of the features mentioned in the figures. The ability to distinguish the variety of structures and features has enabled interpretations to be made on the defining features of the salt and therefore can be used as a reference when working

in similar salt basins. The continual advancements will enable the accurate placement of the reservoir along with the other key features in a petroleum system.

Two major provinces are identified, a salt stock canopy and a complex secondary minibasin province. The control on the structural style above the salt is controlled by two mechanisms, the availability of salt from the original autochthonous salt and the sedimentary loading on the salt canopy. Deformation of the top of the salt is also a result of the overlying strata causing the mobile shale layer located above the salt canopy to become mobilized or incased in the salt canopy.

Mobile shales are commonly found in settings alongside salt bodies because they both are weak ductile materials that form diapirs (Hudec et al., 2023). The criteria needed for the development of mobile shales are a thick salt sequence and a thick rapidly deposited mud prone section, both conditions are met in the GOMB and visible in our AOI. Here we find the detachment of the Eocene-Oligocene salt. The shortening events of the Oligocene- Miocene overlap result in thrusting resulting in folding cored by the mobile shales as seen on flanking the seaward side of minibasin 4. Areas where mobile shale has diminished or is thin relative to the areas containing mobile shale show a chaotic top surface and increased seismic reflections in the salt that are interpreted as being sutures.

The use of 3D seismic along with well data to interpret the salt body, salt weld locations, feeder flank geometry, structural styles located above suprasalt, and interpreted stratal orientation of subsalt sediments in areas of seismic washout zone. Future studies

can use the novel approach taken here with use of high-resolution 3D seismic data sets.

The use of more wells in the area can aid in the validity of the interpretations.

10. REFERENCES

- Arfai, J., Lutz, R., Franke, D., Gaedicke, C., & Kley, J. (2016). Mass-transport deposits and reservoir quality of upper cretaceous chalk within the German central Graben, North Sea. *International Journal of Earth Sciences*, 105, 797-818.
- BOEM (2017). Gulf of Mexico Leasing Maps. Accessed on Dec 5, 2022 from <https://www.boem.gov/sites/default/files/oil-and-gas-energy-program/Mapping-and-Data/Gulf-of-Mexico-OPD-Index-2017.pdf>.
- Boswell, R., Frye, M., Shelandier, D., Shedd, W., McConnell, D. R., & Cook, A. (2012). Architecture of gas-hydrate-bearing sands from Walker Ridge 313, Green canyon 955, and Alaminos canyon 21: northern deepwater Gulf of Mexico. *Marine and Petroleum Geology*, 34(1), 134-149.
- Bowling, J., Ji, S., Lin, D., Reasnor, M., Staines, M., & Burke, N. (2009). From isotropic to anisotropic: Puma/Mad Dog wide azimuth data case study. In *SEG Technical Program Expanded Abstracts 2009* (pp. 246-250). Society of Exploration Geophysicists.
- Bureau of Ocean Energy Management. (2024). Northern GOM Deepwater Bathymetry Grid & 3D Seismic [Map]. BOEM. Retrieved from <https://www.boem.gov/oil-gas-energy/mapping-and-data/map-gallery/northern-GOM-deepwater-bathymetry-grid-3d-seismic>
- Callot, J. P., Salel, J. F., Letouzey, J., Daniel, J. M., & Ringenbach, J. C. (2016). Three-dimensional evolution of salt-controlled minibasins: Interactions, folding, and megaflap development. *Aapg Bulletin*, 100(9), 1419-1442.
- Campbell, D. C. (2005). *Major Quaternary mass-transport deposits in southern Orphan Basin, offshore Newfoundland and Labrador* (p. 10). Natural Resources Canada, Geological Survey of Canada.
- Diegel, F. A., Karlo, J. F., Schuster, D. C., Shoup, R. C., & Tauvers, P. R. (1995). Cenozoic structural evolution and tectono-stratigraphic framework of the northern Gulf Coast continental margin. *AAPG Bulletin*, AAPG Memoir 65, 109-151
- Dooley, T. P., Hudec, M. R., & Jackson, M. P. (2012). The structure and evolution of sutures in allochthonous salt. *AAPG Bulletin*, 96(6), 1045-1070

- Dott Jr, R. H. (1963). Dynamics of subaqueous gravity depositional processes. *AAPG Bulletin*, 47(1), 104-128.
- Durham, L. S., & Correspondent, E. X. P. L. O. R. E. R. (2010). Advancements push 'salt' plays. *AAPG Explorer*, 31(2), 20-24.
- Erlich, R. N., Hale-Erlich, W. S., Pindell, J., Saylor, J. E., & O'Sullivan, P. (2022). Age and provenance of the Middle Jurassic Norphlet Formation of south Texas: stratigraphic relationship to the Louann Salt and regional significance. *Journal of the Geological Society*, 179(6), jgs2022-009.
- Ewing, T. E., & Galloway, W. E. (2019). Evolution of the northern Gulf of Mexico sedimentary basin. In *The sedimentary basins of the United States and Canada* (pp. 627-694). Elsevier.
- Fisher, C., Roberts, H., Cordes, E., & Bernard, B. (2007). Cold seeps and associated communities of the Gulf of Mexico. *Oceanography*, 20(4), 118-129.
- Flinch, J. F., & Soto, J. I. (2022). Structure and Alpine tectonic evolution of a salt canopy in the western Betic Cordillera (Spain). *Marine and Petroleum Geology*, 143, 105782.
- Fiduk, J. C., Weimer, P., Trudgill, B. D., Rowan, M. G., Gale, P. E., Phair, R. L., ... & Queffelec, T. A. (1999). The Perdido Fold Belt, northwestern deep Gulf of Mexico, part 2: seismic stratigraphy and petroleum systems. *AAPG Bulletin*, 83(4), 578-612.
- Fossen, H. (2010). Salt tectonics. *Structural Geology*, 371-394.
- Galloway, W. E. (2001). Cenozoic evolution of sediment accumulation in deltaic and shore-zone depositional systems, northern Gulf of Mexico Basin. *Marine and Petroleum Geology*, 18(10), 1031-1040.
- Galloway, W. E., Whiteaker, T. L., & Ganey-Curry, P. (2011). History of Cenozoic North American drainage basin evolution, sediment yield, and accumulation in the Gulf of Mexico basin. *Geosphere*, 7(4), 938-973.
- Galloway, W.E., 2005, Cenozoic evolution of the northern Gulf of Mexico continental margin, in Gulf Coast Section SEPM 25th Annual Research Conference Proceedings, p. 1–15.
- Galloway, W. E. (2008). Depositional evolution of the Gulf of Mexico sedimentary basin. *Sedimentary basins of the world*, 5, 505-549.

- Galloway, W. E., Ganey-Curry, P. E., Li, X., & Buffler, R. T. (2000). Cenozoic depositional history of the Gulf of Mexico basin. *AAPG Bulletin*, 84(11), 1743-1774.
- Gulf of Mexico Index Map, <https://www.boem.gov/sites/default/files/oil-and-gas-energy-program/Mapping-and-Data/Gulf-of-Mexico-OPD-Index-2017.pdf> (Accessed January 2023)
- Giles, K. A., & Rowan, M. G. (2012). Concepts in halokinetic-sequence deformation and stratigraphy. *Geological Society, London, Special Publications*, 363(1), 7-31.
- Hearon IV, T. E. (2013). Analysis of salt-sediment interaction associated with steep diapirs and allochthonous salt: Flinders and Willouran ranges, south Australia, and the deepwater northern Gulf of Mexico. Colorado School of Mines.
- Hudec, M. R., & Jackson, M. P. (2007). Terra infirma: Understanding salt tectonics. *Earth-Science Reviews*, 82(1-2), 1-28.
- Hudec, M. R., & Jackson, M. P. (2009). Interaction between spreading salt canopies and their peripheral thrust systems. *Journal of Structural Geology*, 31(10), 1114-1129.
- Hudec, M. R., & Jackson, M. (2011). The Salt Mine: A Digital Atlas of Salt Tectonics. *University of Texas at Austin. Bureau of Economic Geology. AAPG Memoir 99*, 10-244
- Hudec, M. R., Norton, I. O., Jackson, M. P., & Peel, F. J. (2013). Jurassic evolution of the Gulf of Mexico salt basin. *AAPG Bulletin*, 97(10), 1683-1710.
- Hudec, M. R., Peel, F. J., Soto, J. I., & Apps, G. M. (2023). Interaction between salt and mobile shale in the East Breaks foldbelt, northwestern Gulf of Mexico. *Marine and Petroleum Geology*, 155, 106391.
- Hung, B., & Yin, Y. (2012). Optimal stacking for multi-azimuth pre-stack seismic data. *ASEG Extended abstracts*, 2012(1), 1-4.
- Hunt, B. W. (2013). *Regional Norphlet facies correlation, analysis and implications for paleostructure and provenance, eastern Gulf of Mexico*. The University of Alabama. ProQuest Dissertations & Theses, 2013. 1539948
- Jackson, M. P., & Hudec, M. R. (2017). Salt tectonics: Principles and practice. Cambridge University Press. <https://doi.org/10.1017/9781139003988>

- Jackson, M. P. A., & Cramez, C. (1989). Seismic recognition of salt welds in salt tectonics regimes (abs). SEPM Gulf Coast Section, 10th Annual Research Conference, Program and Extended Abstracts, Houston Texas, 66-71
- Jones, I. F., & Davison, I. (2014). Seismic imaging in and around salt bodies. *Interpretation*, 2(4), SL1-SL20.
- Callot, J. P., Salel, J. F., Letouzey, J., Daniel, J. M., & Ringenbach, J. C. (2016). Three-dimensional evolution of salt-controlled minibasins: Interactions, folding, and megaflap development. *AAPG Bulletin*, 100(9), 1419-1442.
- Kopaska-Merkel, D. C., Mann, S. D., & Tew, B. H. (1992). *Geologic setting, petrophysical characteristics, and regional heterogeneity patterns of the Smackover in southwest Alabama. Draft topical report on Subtasks 2 and 3* (No. DOE/BC/14425-T11). Alabama Geological Survey, Tuscaloosa, AL (United States).
- Lesh, B. (2022). Geochemical Characterization of the Louann Salt, Puma Field, Green Canyon, Gulf of Mexico Basin—Using XRF and XRD. Stephen F. Austin State University. Master's Thesis.
- Martinez, G. O., Sawyer, D. E., & Portnov, A. (2024). Seismic geomorphology of the Chandeleur submarine landslide in the northern Gulf of Mexico. *Geological Society, London, Special Publications*, 525(1), SP525-2021.
- Mattson, A. (2019). Application of 3D Salt Modeling: An Example from the Northeastern Gulf of Mexico. Masters These & Specialist Projects. Paper 3157
- Mancini, E. A., Mink, R. M., Bearden, B. L., & Wilkerson, R. P. (1985). Norphlet Formation (Upper Jurassic) of southwestern and offshore Alabama: environments of deposition and petroleum geology. *AAPG Bulletin*, 69(6), 881-898.
- Mancini, E. A., Tew, B. H., & Mink, R. M. (1990). Jurassic sequence stratigraphy in the Mississippi interior salt basin of Alabama, 40, 521-529
- Mancini, E.A., M. Badali, T.M. Puckett, J.C. Llinas, and W.C. Parcell, 2001, Mesozoic carbonate petroleum systems in the northeastern Gulf of Mexico area, in *Petroleum Systems of Deep-Water Basins: GCS-SEPM Foundation 21st Annual Research Conference*, 423-451.

- Mattson, A. G., Gani, M. R., Roesler, T., Gani, N. D., & Ford, J. T. (2020). 3D mapping of intruding salt bodies in the subsurface of the Gulf of Mexico using 3D seismic data. *Results in Geophysical Sciences*, 1, 100004.
- Méndez-Hernández, E. (2008). *Integrating sequence stratigraphy and seismic attributes for quantitative reservoir characterization: A case study of a Pliocene reservoir, Campeche Sound, Mexico*. The University of Oklahoma. ProQuest Dissertations & Theses, 2008. 3336783
- Nardin, T. R., Hein, F. J., Gorsline, D. S., & Edwards, B. D. (1979). A review of mass movement processes, sediment and acoustic characteristics, and contrasts in slope and base-of-slope systems versus canyon-fan-basin floor systems, 27(1), 61-73.
- Nikolinakou, M. A., Heidari, M., Hudec, M. R., & Flemings, P. B. (2017). Initiation and growth of salt diapirs in tectonically stable settings: Upbuilding and megaflaps. *AAPG Bulletin*, 101(6), 887-905.
- Omosanya, K. O., & Harishidayat, D. (2019). Seismic geomorphology of Cenozoic slope deposits and deltaic clinoforms in the Great South Basin (GSB) offshore New Zealand. *Geo-Marine Letters*, 39(1), 77-99.
- Pashin, J., Guohai, J., & Hills, D. (2016). *Mesozoic structure and petroleum systems in the DeSoto Canyon Salt Basin in the Mobile, Pensacola, destin Dome, and Viosca Knoll areas of the MAFLA shelf* (No. DOE-SSEB-0026086-43). Southern States Energy Board, Peachtree Corners, GA (United States).
- Peel, F. J. (2014). How do salt withdrawal minibasins form? Insights from forward modeling, and implications for hydrocarbon migration. *Tectonophysics*, 630, 222-235.
- Pepper, F. (1982). Depositional Environments of the Norphlet Formation (Jurassic) for Southwestern Alabama, 32(1), 17-22.
- Pilcher, R. S., Kilsdonk, B., & Trude, J. (2011). Primary basins and their boundaries in the deep-water northern Gulf of Mexico: Origin, trap types, and petroleum system implications. *AAPG Bulletin*, 95(2), 219-240.
- Prather, B. E., Booth, J. R., Steffens, G. S., & Craig, P. A. (1998). Classification, lithologic calibration, and stratigraphic succession of seismic facies of intraslope basins, deep-water Gulf of Mexico. *AAPG Bulletin*, 82(5), 701-728.

- Posamentier, H. W., & Kolla, V. (2003). Seismic geomorphology and stratigraphy of depositional elements in deep-water settings. *Journal of sedimentary research*, 73(3), 367-388.
- Rowan, M. G., & Giles, K. A. (2021). Passive versus active salt diapirism. *AAPG Bulletin*, 105(1), 53-63.
- Rowan, M. G., Peel, F. J., & Vendeville, B. C. (2004). Gravity-driven fold belts on passive margins. *AAPG Bulletin*, 88(4), 475-494.
- Rowan, M. G., & Weimer, P. (1998). Salt-sediment interaction, northern Green Canyon and Ewing bank (offshore Louisiana), northern Gulf of Mexico. *AAPG Bulletin*, 82(5), 1055-1082.
- Sawyer, D. E., Flemings, P. B., Dugan, B., & Germaine, J. T. (2009). Retrogressive failures recorded in mass transport deposits in the Ursa Basin, Northern Gulf of Mexico. *Journal of Geophysical Research: Solid Earth*, 114(B10).
- Soto, J. I., Heidari, M., & Hudec, M. R. (2021). Proposal for a mechanical model of mobile shales. *Scientific Reports*, 11(1), 23785.
- Snedden, J. W., & Galloway, W. E. (2019). *The Gulf of Mexico sedimentary basin: Depositional evolution and petroleum applications*. Cambridge University Press.
- Snedden, J. W., Norton, I., Hudec, M., Eljalafi, A., & Peel, F. (2018). Paleogeographic Reconstruction of the Louann Salt Basin in the Gulf of Mexico. In *AAPG ACE 2018*.
- Talbot, C. J., Rönnlund, P., Schmeling, H., Koyi, H., & Jackson, M. P. A. (1991). Diapiric spoke patterns. *Tectonophysics*, 188(1-2), 187-201.
- Ward, C. H., & Tunnell, J. W. (2017). Habitats and biota of the Gulf of Mexico: an overview. *Habitats and biota of the Gulf of Mexico: before the Deepwater Horizon oil spill*, 1-54.
- Weiland, R. J., Adams, G. P., McDonald, R. D., Rooney, T. C., & Wills, L. M. (2008, May). Geological and biological relationships in the Puma appraisal area: From salt diapirism to chemosynthetic communities. In *Offshore Technology Conference* (pp. OTC-19360). OTC.
- Weimer, P., & Shipp, C. (2004). Mass transport complex: Musing on past uses and suggestions for future directions. In *Offshore Technology Conference* (pp. OTC-16752). OTC.

- Winker, C. D. (1982). Cenozoic shelf margins, northwestern Gulf of Mexico. *GCAGS Transactions*, 32, 427-444.
- Wu, S., Vail, P. R., & Cramez, C. (1990). Allochthonous salt, structure and stratigraphy of the north-eastern Gulf of Mexico. Part I: Stratigraphy. *Marine and Petroleum Geology*, 7(4), 318-333.
- Wu, N., Jackson, C. A. L., Johnson, H. D., Hodgson, D. M., & Nugraha, H. D. (2020). Mass-transport complexes (MTCs) document subsidence patterns in a northern Gulf of Mexico salt minibasin. *Basin Research*, 32(6), 1300-1327.
- Yang, L., & Sun, S. Z. (2020). Seismic horizon tracking using a deep convolutional neural network. *Journal of Petroleum Science and Engineering*, 187, 106709.

11.Vita

Rodrigo Velasquez was born in San Felipe, Guanajuato, moved to Mineral Wells Texas where he graduated from Mineral Wells High School June 2015. Starting his college journey at Weatherford College where he graduated with an Associate in Arts in May 2018. Rodrigo then proceeded to attend Tarleton State University where he received his Bachelor of Science in Geoscience in December 2020. He then proceeded to enroll in graduate studies at Stephen F. Austin State University and received the degree of Master of Science in Geology in August 2024.

Permanent Address: 850 Millsap Hwy, Mineral Wells TX, 76067

Style Manual Designation: Geological Society of America

This thesis was written by Rodrigo Velasquez